

# A coupled atmosphere-ocean model for transient climate change studies

Gary L. Russell , James R. Miller & David Rind

**To cite this article:** Gary L. Russell , James R. Miller & David Rind (1995) A coupled atmosphere-ocean model for transient climate change studies, *Atmosphere-Ocean*, 33:4, 683-730, DOI: [10.1080/07055900.1995.9649550](https://doi.org/10.1080/07055900.1995.9649550)

**To link to this article:** <http://dx.doi.org/10.1080/07055900.1995.9649550>



Published online: 19 Nov 2010.



Submit your article to this journal 



Article views: 694



View related articles 



Citing articles: 154 View citing articles 

---

# A Coupled Atmosphere-Ocean Model for Transient Climate Change Studies

Gary L. Russell, James R. Miller<sup>1</sup> and David Rind

NASA/Goddard Space Flight Center

Institute for Space Studies

2880 Broadway, New York, NY 10025

[Original manuscript received 2 September 1994; in revised form 10 March 1995]

---

**ABSTRACT** A new coupled atmosphere-ocean model has been developed for climate predictions at decade to century scales. The atmospheric model is similar to that of Hansen et al. (1983) except that the atmospheric dynamic equations for mass and momentum are solved using Arakawa and Lamb's (1977) C grid scheme and the advection of potential enthalpy and water vapour uses the linear upstream scheme (Russell and Lerner, 1981). The new global ocean model conserves mass, allows for divergent flow, has a free surface and uses the linear upstream scheme for the advection of potential enthalpy and salt. Both models run at  $4^\circ \times 5^\circ$  resolution, with 9 vertical layers for the atmosphere and 13 layers for the ocean. Twelve straits are included, allowing for subgrid-scale water flow. Runoff from land is routed into appropriate ocean basins. Atmospheric and oceanic surface fluxes are of opposite sign and are applied synchronously. Flux adjustments are not used. Except for partial strength alternating binomial filters (Shapiro, 1970), which are applied to the momentum components in the atmosphere and oceans, there is no explicit horizontal diffusion.

A 120-year simulation of the coupled model starting from the oceanic initial conditions of Levitus (1982) is discussed. The model dynamics stabilize after several decades. The maximum northward ocean heat flux is  $1.4 \times 10^{15} \text{ W}$  at  $16^\circ\text{N}$ . The model appears to maintain the vertical gradients characterizing the separation between the upper and deep ocean spheres. Inadequacies in the coupled model simulation lead to decreasing temperature and salinity in the high latitude North Atlantic and to a poor simulation of the northern North Atlantic thermohaline circulation. The mass transport of the Gulf Stream is about half of observed values, while the transports of the Kuroshio and Antarctic Circumpolar Currents are similar to observations. Additional deficiencies include a climate drift in the surface air temperature of  $0.006^\circ\text{C year}^{-1}$  due to a radiation imbalance of  $7.4 \text{ W m}^{-2}$  at the top of the atmosphere and too warm temperatures in the eastern portions of tropical oceans. The coupled model should be useful for delineating modelling capabilities without the use of flux adjustments and should serve as a benchmark for future model improvements.

**RÉSUMÉ** On a élaboré un nouveau modèle couplé atmosphère-océan de prévisions du climat aux échelles allant de la décennie au siècle. Ce modèle atmosphérique est semblable à celui de Hansen et al. (1983) sauf que les équations dynamiques atmosphériques pour la masse et la quantité de mouvement sont calculées à l'aide du schéma de grille C d'Arakawa et

---

<sup>1</sup>Department of Marine and Coastal Sciences, Cook College, Rutgers University, New Brunswick, NJ 08903

*Lamb (1977) et que l'advection d'enthalpie potentielle et d'eau vapeur utilise le schéma linéaire vers la source (Russell et Lerner, 1981). Le nouveau modèle océanique global conserve la masse, permet une circulation divergente, contient une surface libre, et utilise le schéma linéaire vers la source pour l'advection de l'enthalpie potentielle et du sel. Les deux modèles ont une résolution de  $4^\circ \times 5^\circ$  et neuf couches verticales pour l'atmosphère et treize pour l'océan. Douze détroits sont inclus permettant une circulation d'eau sous-grille. L'écoulement des terres est dirigé vers les bassins océaniques pertinents. Les flux de surface, océanique et atmosphérique, sont de signe opposés et synchroniques. On n'ajuste pas les flux. Sauf pour des filtres binomiaux de force partielle alternant (Shapiro, 1970), appliqués aux composants de la quantité de mouvement dans l'atmosphère et l'océan, il n'y a pas de diffusion horizontale explicite.*

*On étudie une simulation de 120 années d'un modèle couplé des conditions océaniques initiales de Levitus (1982). La dynamique du modèle se stabilise après plusieurs décennies. Le flux maximal de chaleur vers le nord est de  $1,4 \times 10^{15} \text{ W}$  à  $16^\circ$ . Le modèle semble maintenir les gradients verticaux qui caractérisent la séparation entre les couches supérieures et profondes de l'océan. Des différences dans la simulation du modèle couplé entraînent, dans l'Atlantique Nord, une diminution de la température et de la salinité dans les hautes latitudes, et une piètre simulation de la circulation thermale. Le transport de masse du Gulf Stream est environ la moitié des valeurs observées alors que les transports des courants Kuroshio et Circumpolaire Antarctique sont semblables aux observations. Les différences supplémentaires comprennent une dérivation du climat pour la température de l'air en surface ( $0,006^\circ\text{C a}^{-1}$ ) entraînée par un rayonnement inégal de  $7,4 \text{ W m}^{-2}$  au sommet de l'atmosphère, et des températures trop chaudes sur les secteurs est des océans tropicaux. Le modèle couplé devrait être utile pour cadrer les possibilités de modélisation sans les ajustements de flux et pourrait servir de seuil pour les améliorations futures.*

## 1 Introduction

Global atmospheric general circulation models (AGCMs) have been used extensively to simulate the Earth's present climate with reasonable success. AGCMs also have been used to estimate climate changes that might occur by adding greenhouse gases to the atmosphere. Because the poleward heat transport by the ocean circulation is comparable to that by the atmospheric circulation, climate change simulations with AGCMs need some technique to incorporate ocean heat transport in order for the control run to produce reasonable simulations of the current climate. Two techniques have been used extensively in this regard.

In the first technique, ocean heat transports are specified and remain invariant in both the control and climate change experiment. Russell et al. (1985) ran the Goddard Institute for Space Studies (GISS) AGCM with climatologically specified ocean surface temperatures and sea ice distributions, and for each grid box derived the daily converged ocean heat transport necessary to maintain the current climate. Hansen et al. (1984, 1988) incorporated these converged ocean heat transports with the same AGCM to estimate the climate response to doubling of atmospheric carbon dioxide and the climate response to three greenhouse gas scenarios in transient simulations. They were able to estimate three principal feedback factors, water vapour, snow-ice albedo and cloud cover that drive the global temperature change.

The use of specified ocean heat transports prevented them from estimating the ocean circulation feedback factor, which may be of the same order. Numerous other groups have now used this approach, which is sometimes called the "q-flux" technique.

A more complete approach is to couple the atmosphere to a dynamic ocean in which transports are allowed to vary. The International Panel on Climate Change (IPCC, 1992), and the World Climate Research Programme (WCRP) (Gates et al., 1993) have summarized efforts to use fully coupled dynamic atmosphere-ocean models, and the IPCC is currently collecting data from additional efforts. The problem is complicated by the inability of coupled models to produce a realistic representation of the present climate without help, i.e., without some incorporation of specified heat and fresh water fluxes. The inclusion of these flux adjustments, which are unchanged in the experiment and control and are of comparable magnitude to the total flux used by Hansen et al. (1984) (see Sausen et al., 1988; and Manabe et al., 1991), provides a limitation on estimating the ocean circulation feedback, although more flexibility exists than with the previous "q-flux" approach.

Gates et al. (1993) recommend "that further study be made of the systematic errors of coupled ocean-atmosphere models both with and without flux adjustments". To that end we describe in this paper a new coupled atmosphere-ocean model which is run without flux adjustment. The model is integrated for 120 years starting from the climatological initial conditions of Levitus (1982). We discuss the model formulation, including specific features unique to this effort. We show how the model departs as a function of time away from the initial conditions, and present the relevant oceanic, thermodynamic and hydrological simulations. We anticipate that this version will be useful as a benchmark for further coupled model development.

## 2 Formulation of the Coupled Atmosphere-Ocean Model

### a Atmospheric model

The atmospheric model, run at  $4^\circ \times 5^\circ$  horizontal resolution with nine layers in the vertical (in  $\sigma$ , or "terrain-following" coordinates), is a variant of the version published by Hansen et al. (1983) (henceforth called "Model II"). As the results from this model have been discussed in detail, we concentrate on the changes incorporated in this version of the coupled model. A summary of the changes is presented in Table 1.

The atmospheric mass and momentum equations are solved on a modified version of the "C grid" scheme of Arakawa and Lamb (1977) instead of the "B grid" as was formerly done. An advantage of this shift is that it allows the atmosphere model to be consistent with the ocean model. In the C grid the zonal velocity is defined between two adjacent east-west grid boxes, and the meridional velocity is defined between two adjacent north-south grid boxes. This proves ideal for handling the coast lines in the ocean, as the flow perpendicular to the coast line is set to zero and the flow parallel to the coast is always one-half grid box away. An additional

TABLE 1. Summary of changes in atmospheric component of coupled model from Model II (Hansen et al., 1983).

- 
- Directional gradients of heat and water vapour are prognostic
  - Linear upstream scheme (Russell and Lerner, 1981) used for advection of heat and water and water vapour
  - Momentum equation uses C grid scheme (Arakawa and Lamb, 1977)
  - Moist convection and large-scale condensation performed on horizontal quarter box resolution
  - Simplified planetary boundary layer scheme
  - Cloud optical thicknesses depend on amount of condensate
- 

advantage is that the C grid provides a more realistic computation of geostrophic adjustment, with better gravity wave propagation. A disadvantage is that it produces two grid point noise in the wind field, which has to be controlled by filtering the winds at all levels. In this model we use one-dimensional, eighth-order alternating binomial filters in both the zonal and meridional wind directions (Shapiro, 1970).

In addition to calculating the mean (potential) temperature and moisture in each grid box, the model also calculates the gradient of these fields as prognostic variables. This is done by using the "linear upstream scheme" (Russell and Lerner, 1981) for heat and moisture advection, with subgrid-scale linear gradients in three dimensions. The numerical scheme produces significantly smoother patterns than the second-order advection used in Model II; it is weakly diffusive, but comparisons with a "quadratic upstream scheme" (Prather, 1986), which is less diffusive, show little difference in the resulting dynamic and thermodynamic properties. The calculation of the linear gradient allows subgrid-scale effects to be included in the physics. For example, convection is done on quarter grid boxes, by assessing the moist static energy profile (a function of temperature and moisture, each of which is known on quarter grid resolution). Hence, the resolution for specific physics subroutines occurs on a finer scale than indicated by the grid box resolution alone.

The atmospheric boundary layer has been replaced by a simplified version, in which surface air quantities are linearly related to values in the first full atmospheric layer and its vertical gradients; the cross-isobar angle is determined from observations and the calculated Richardson number (a function of vertical stability and wind shear). The formulation used in Model II had an inappropriate dependence on the Ekman length near the equator, where the reciprocal of the sine of latitude becomes very large, making the upper boundary condition for the wind profile impossible to satisfy. The simplified scheme corrected a low-latitude precipitation problem induced by this error. It also reduced ground temperature oscillations through the use of an improved implicit time scheme.

The radiation scheme used in the model is the same as in Model II, except that the optical depths for cloud cover were altered so as to provide a better agreement with observations of solar radiation at the surface. The major discrepancy occurred at low latitudes, where the optical depths appeared to be too small; the correction involved relating optical depth to precipitation/moisture loading. Comparison with the International Satellite Cloud Climatology (ISCCP) data (Tselioudis et al., 1992)

TABLE 2. Primary features of the ocean component of coupled model.

- 
- Directional gradients of heat and salt are prognostic
  - Linear upstream scheme used for advection of heat and salt
  - Momentum equation uses new C grid scheme
  - Alternating binomial filter applied to momentum components
  - No horizontal diffusion of heat or salt
  - Free surface, divergent flow allowed
  - Sea water mass is conserved, not volume
  - Up to 13 vertical layers of approximate thicknesses 12, 18, 27, 41, 61, 91, 137, 205, 308, 461, 692, 1038, 1557 metres
  - Vertical diffusion has Richardson number dependence on horizontal quarter box resolution
  - Nonentraining convection on horizontal quarter box resolution
  - 12 subgrid straits included
- 

implies that this formation, a variant of which is used by other modelling groups (e.g. Boer et al., 1992), should probably be revised. It will affect the climate sensitivity of the model.

Extensive comparisons were conducted of the atmospheric model, using specified climatological sea surface temperatures, with Model II (at  $4^\circ \times 5^\circ$  resolution). In general, the new model climatology was similar to, or more accurate than, that of Model II when compared with observations (e.g. Druyan et al., 1994). Additional atmospheric model developments at GISS, for example, a new land surface scheme, will ultimately be included into the coupled model.

### **b Ocean model**

The ocean model is completely new, having been generated specifically to be used in coupled atmosphere-ocean studies. Its primary features are listed in Table 2. The model uses Arakawa's C-grid, while modifying the solution for the momentum equation. Only two mass boxes on either side of a velocity point are used to calculate momentum, as opposed to six mass boxes in the Arakawa and Lamb (1977) scheme. This reduction was due to the problems caused by having surrounding land boxes with no ocean mass, primarily in the Arctic Ocean. In conjunction with the use of the C-grid, one-dimensional, eighth order alternating binomial filters (Shapiro, 1970) are incorporated that properly handle coast lines and the poles.

The model is run at  $4^\circ \times 5^\circ$  resolution with the linear upstream scheme used for potential enthalpy and salt advection. Potential enthalpy is the prognostic variable rather than potential temperature as it accounts for variations in specific heat capacity (a function of temperature and salinity).

The model is run with a maximum of 13 layers in the vertical, but the actual number depends on the horizontal location: the bottom topography under the oceans is adjusted to be at depths in metres of  $-24(1.5^L - 1)$  where L is the number of layers in the ocean column. The ratio of an ocean grid box mass to the grid box mass below is 2/3, so the standard resolution thicknesses are approximately 12, 18, 27, 40.5, 61, 91, 137, 205, 308, 461, 692, 1038 and 1557 metres. Hence layers either exist in full or not at all, eliminating the need for  $\sigma$  or terrain-following

## Ocean Layers for the Atmosphere-Ocean Model

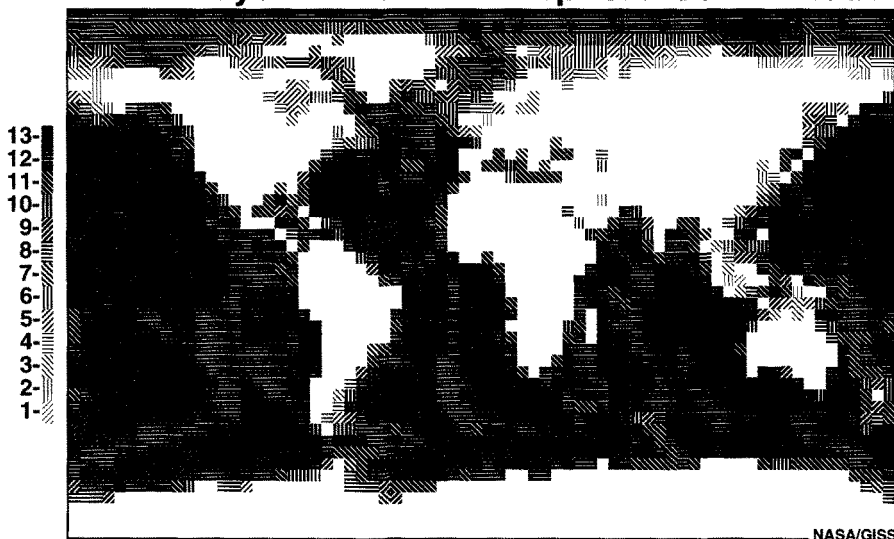


Fig. 1 Number of ocean vertical layers for each horizontal grid column for the standard  $4^\circ \times 5^\circ$  resolution.

coordinates, which impose difficulties in solving for the pressure gradient force. Thus the vertical coordinate is mass per unit area, including the masses of air, ice and water (with constant gravity, this is equivalent to using pressure as the vertical coordinate). As noted above, the calculation of the three-dimensional gradients in addition to the mean quantities effectively provides for increased resolution, in both the horizontal and vertical dimensions, which is subsequently used in the ocean model physics as well.

Fig. 1 shows the number of ocean vertical layers in each grid box. The Central American isthmus and the Malaysian peninsula and the islands south of it have been filled in, and a northwest passage between North America and Greenland has been opened. Large islands have been retained.

The physics incorporated in the ocean includes convection, vertical diffusion and bottom friction. For convection, the vertical structure of potential specific volume is checked on each horizontal quarter box ocean column, and if it is found to be unstable (i.e. if potential specific volume increases with depth) then nonentraining convection occurs. One-eighth of the quarter grid box mass (hence 1/32 of the grid box mass) is mixed to a depth determined by the vertical profile. Use is made of the vertical gradients for temperature and salinity in this calculation. Convection mixes mass, potential enthalpy, salt and momentum.

As with convection, vertical mixing (diffusion) is performed on horizontal quarter boxes. Diffusion is applied between each adjacent pair of layers in the vertical. A single diffusion coefficient is applied to momentum, potential enthalpy and salt:

$$\kappa(\text{cm}^2 \text{ s}^{-1}) = 3.76/(0.5 + 2Ri^2) \quad (1)$$

which depends on the Richardson number,  $Ri$ , calculated by vertical differences as:

$$Ri = -\Delta\beta\Delta P / [(\Delta u)^2 + (\Delta v)^2] \quad (2)$$

where  $\beta$  is the potential density,  $P$  is the pressure, and  $u$  and  $v$  are the eastward and northward velocity components. Table 3 compares the diffusion coefficient for the current model with that used in some other models. Shown in Table 3a is a comparison, based explicitly on the  $Ri$  number formula, with the coefficients used by Pacanowski and Philander (1981) for the tropical ocean. In Table 3b a comparison is given of the model's effective diffusion values as a function of depth with the values as a function of depth used by Bryan and Lewis (1979) for the global ocean (see also Jiang and Fung, 1994), and with the values used by Washington and Meehl (1989). In general, the vertical diffusion is less in this model, sometimes by a considerable magnitude, except it is greater in the first 50 m than that used by Bryan and Lewis (1979). Note also that this model does not employ explicit horizontal diffusion for momentum, heat or salt, in contrast to values of  $10^7$  to  $10^9$   $\text{cm}^2 \text{ s}^{-1}$  which are commonly used in other models (Washington and Meehl, 1989; Jiang and Fung, 1994). The ability to eliminate the need for numerical diffusion is believed to be a direct consequence of the more accurate horizontal advection scheme for heat and salt.

The ocean velocity of the lowest layer of each ocean column is reduced in order to simulate bottom friction. The bottom drag vector is

$$\tau_b(\text{kg m}^{-1} \text{ s}^{-2}) = \rho C_d |(u, v)|(u, v) \quad (3)$$

where  $C_d$  is a dimensionless drag coefficient,  $\rho$  ( $\text{kg m}^{-3}$ ) is density, and  $(u, v)$  is velocity.  $\rho C_d$  is set to  $1 \text{ kg m}^{-3}$ .

About 70% of the kinetic energy produced by the atmospheric stress is destroyed by convection and vertical mixing. The destruction of kinetic energy by bottom friction is very small, amounting to about 1%.

Given the relatively coarse horizontal resolution in the ocean model, it was necessary to incorporate straits in the model so as to allow for passage of water through grid boxes which would otherwise be classified as all land. Straits are arrays with one vertical dimension. The mass of water in a strait is nondivergent. The mass flux is dynamically accelerated only by the pressure gradient force between the whole ocean grid boxes at each end. Advection of potential enthalpy and salt through a strait follows the basic principles of the linear upstream scheme. Convection and vertical diffusion are applied to the two halves of each strait in the same way they are applied to the quarter boxes of whole ocean grid boxes. Bottom friction with the same coefficient is applied in the lowest layer in each strait.

Twelve straits are included in the model. The relevant parameters are shown in Table 4. Note that the straits through the Indonesian Archipelago are represented in the model as whole grid boxes, so a special strait classification is not needed.

When energy losses cause the first layer of the open ocean to cool below the freezing point, the ocean stays at the freezing point and 0.5 m thick sea ice is

TABLE 3a. Ocean vertical diffusion coefficients ( $\text{cm}^2/\text{s}$ ) for the coupled model and those of Pacanowski and Philander (1981).

Richardson number	Coupled model	Pacanowski momentum	Pacanowski heat & salt
0.0	7.53	51.00	51.10
0.125	7.08	19.93	12.37
0.25	6.02	10.87	4.93
0.375	4.82	7.05	2.55
0.5	3.76	5.08	1.55
0.75	2.32	3.21	0.78
1.0	1.51	2.39	0.50
2.0	0.84	1.41	0.23
4.0	0.23	1.11	0.15
8.0	0.06	1.03	0.13

TABLE 3b. Effective global annual vertical diffusion coefficients ( $\text{cm}^2/\text{s}$ ) for years 88–97 of the coupled model simulation and an evaluation of the vertical diffusion coefficient formula for heat and salt of Bryan and Lewis (1979) as a function of depth (m). Bryan and Lewis used  $1 \text{ cm}^2/\text{s}$  as the vertical viscosity for momentum. Washington and Meehl (1989) used  $1 \text{ cm}^2/\text{s}$  as the vertical diffusion coefficient for heat and salt and for vertical viscosity they used  $10 \text{ cm}^2/\text{s}$  between the upper two layers away from the equator,  $20 \text{ cm}^2/\text{s}$  at the equator, and  $1 \text{ cm}^2/\text{s}$  in the deeper ocean.

Depth	Coupled model	Bryan and Lewis
12	5.464	0.305
30	1.500	0.305
57	0.585	0.305
98	0.277	0.306
158	0.219	0.307
249	0.177	0.308
386	0.176	0.310
591	0.162	0.314
899	0.155	0.321
1360	0.151	0.339
2052	0.146	0.429
3093	0.142	1.205

formed. With additional energy loss the sea ice thickens, as seen in Hansen et al. (1988). Since the model assumes that sea ice contains no salt, the salt concentration of the first ocean layer increases when sea ice forms or thickens.

When surface fluxes, principally insolation, cause the sea ice temperature to rise above  $0^\circ\text{C}$ , the temperature stays at  $0^\circ\text{C}$  and snow or sea ice is melted, which runs into the ocean below. If sea ice becomes thinner than 0.5 m, then it is contracted

TABLE 4. Location and size (metres) of the 12 straits in the atmosphere-ocean model.

Strait	From	To	Depth	Width
Fury & Hecla	87°W, 72°N	82°W, 68°N	30	20000
Nares	71°W, 77°N	64°W, 81°N	158	50000
Gibraltar	6°W, 35°N	0°, 37°N	158	25000
English	0°, 50°N	2°E, 52°N	30	35000
Kattegat	10°E, 58°N	16°E, 56°N	30	60000
Bosphorus	28°E, 40°N	30°E, 41°N	30	6000
Red Sea	39°E, 20°N	40°E, 19°N	249	250000
Bab-al-Mandab	44°E, 16°N	45°E, 14°N	249	25000
Hormuz	55°E, 26°N	61°E, 23°N	30	50000
Malacca	99°E, 4°N	105°E, 2°N	57	50000
Korea	127°E, 36°N	131°E, 36°N	98	170000
Soya-Kaikyo	139°E, 43°N	135°E, 46°N	30	40000

TABLE 5. Coupling procedures.

- Synchronous coupling every hour
- Surface fluxes of water, heat and momentum are applied to atmosphere and ocean with same magnitude but opposite sign
- River flow with proper direction and timing (Miller et al., 1994)
- No surface flux corrections
- No ocean restoring forces

horizontally so that it remains 0.5 m thick. If the temperature of the first ocean layer rises above 0°C, then sea ice is melted vertically and horizontally, drawing the necessary energy from the ocean which cools back to 0°C.

The temperature within the sea ice is determined by a two-layer model. Leads in the sea ice are calculated as was done for Model II (Hansen et al., 1984): the minimum fraction of open ocean area in a grid box is  $0.1(z)^{-1}$ , where  $z$  is the sea ice thickness in metres. Thus as the sea ice thins, leads expand. In the present version of the coupled model, sea ice is not advected. The atmospheric momentum stress on sea ice is passed directly to the ocean model's first layer.

### c Coupling procedures

With  $4^\circ \times 5^\circ$  resolution, both the atmosphere and ocean model are integrated with a dynamics time step of 7.5 minutes. The physics time step for each model is one hour. Thus, the models are truly synchronously coupled. The coupling procedures are summarized in Table 5.

Since the ocean model has a free surface, it allows water mass divergence and direct interaction with the atmosphere. Killworth (1991) discusses the implications of using large-scale, free-surface ocean models and notes that the need for the time-consuming relaxation condition for determining the stream function in the presence of small islands used in rigid-lid models is eliminated. As shown in Fig. 1, numerous islands are included explicitly.

Turbulent transfers of heat, moisture and momentum between the atmosphere and ocean are a function of the wind speed and stability through the dependence of the drag coefficient  $C_d$  on the Richardson number, i.e.:

$$C_d = C_{dN}(0.5 + 2Ri^2)^{-1} \quad (4)$$

Where  $C_{dN}$  is the neutral drag coefficient, a function of the surface wind speed. If the surface layer is unstable, so that the Richardson number is negative, the  $C_d$  is set to  $2C_{dN}$ . The functional relationships for evaporative and sensible heat flux, and surface drag are similar to those in Hansen et al. (1983), although the method of solution uses a more efficient implicit scheme.

Absorbed solar radiation on the open ocean surface penetrates through the first three layers of the ocean according to the formula of Paulson and Simpson (1977). The absorbed insolation affects both the mean and the vertical gradients of potential enthalpy in the ocean.

The atmosphere-ocean model uses river flow to conserve water and to return continental runoff to the oceans. The river direction file and an off-line version of the river routing model are described by Miller et al. (1994). For each continental grid box, the river direction file indicates which of the eight adjacent or diagonal boxes is downstream from the given box, except that some continental boxes have no outlet.

Precipitation runoff over land or land ice, and snow melt in a grid box, immediately increase the river and lake mass of a grid box (i.e. there is no time delay for either surface or ground water flow to reach the rivers and lakes). Precipitation and evaporation on the lake fraction of a continental grid box also increases or decreases the river and lake mass. River and lake mass above the sill depth is passed downstream to lower rivers and lakes and eventually into the ocean. Water mass is conserved globally by river transport.

The river mass flux leaving a grid box to its downstream neighbour is

$$F(\text{kg s}^{-1}) = M u d^{-1} \quad (5)$$

where  $M$  (kg) is the river and lake mass above the sill depth in the box and  $d$  (metres) is the mean distance between a grid box and its downstream neighbour.  $u$  ( $\text{ms}^{-1}$ ) is an effective flow speed which depends on the topography gradient,  $i$ :

$$u = 0.35 i / i_0 \quad (6)$$

where  $i_0 = 0.00005$  is the reference topography gradient.  $u$  is limited to vary between 0.15 and  $5 \text{ ms}^{-1}$ . The values of  $u$  were globally optimized by Miller et al. (1994) so that the fresh water arrives in the proper coastal boxes with the proper seasonal timing. Substantial evaporation on the lake fraction can cause  $M$  to become negative, at which point  $F$  is set to zero.

Each horizontal grid square is either all "land" (which may include ground,

TABLE 6. Prognostic variables for land reservoirs, for sea-ice or lake-ice reservoirs, and for lake and river mass

- 
- Mass of ground liquid waters ( $\text{kg/m}^2$ )
  - Mass of ground solid ice and snow ( $\text{kg/m}^2$ )
  - Temperature of ground ( $^\circ\text{C}$ )
  - Snow mass above glacial ice ( $\text{kg/m}^2$ )
  - Heat, including latent energy, of glacial ice ( $\text{J/m}^2$ )
  - Horizontal ratio of sea ice to ocean
  - Sea ice mass and snow mass above sea or lake ice ( $\text{kg/m}^2$ )
  - Heat, including latent energy, of sea or lake ice ( $\text{J/m}^2$ )
  - Lake and river mass above the sill depth (kg)
- 

glacial ice, open lakes, or lake ice) or all “ocean” (which may include open water or sea ice.) The prognostic variables for the land reservoirs and for sea ice and lake ice reservoirs are given in Table 6. For the standard resolution, these reservoirs contain two vertical layers for mass and heat. Mass of snow contains its own prognostic variable, but the heat content of snow is combined with the heat of the upper layer. Lake temperature and lake ice mass are not prognostic variables, but are specified from climatology. Lake and river mass above the sill depth is prognostic.

#### **d Summary**

The coupled model has several distinctive features. It is truly synchronously coupled, with joint physical processes occurring every hour. The free ocean surface allows for direct interactions between the atmosphere and ocean, including water mass divergence. It also allows the ocean height (sea level) to be calculated directly. Mass, heat and salt are transported through 12 straits that are too small to be resolved by the grid resolution. Continental river flow from the atmospheric model is added to the ocean with proper location and timing.

The use of the linear upstream scheme for advection of heat and salt (or heat and water vapour in the atmosphere) allows the model to calculate both the mean and first-order gradient of these quantities in three dimensions. This approach effectively provides the model finer horizontal and vertical resolution, which is utilized in the physics by calculating subgrid-scale convective fluxes, and sublayer vertical stability profiles. Replacement of the second order heat and moisture/salinity advection schemes, which have been shown to be noisy when mass variations occur between grid boxes (Russell and Lerner, 1981), is likely responsible for the ability of this model to run without using explicit horizontal diffusion for numerical stability. The vertical diffusion is also smaller than commonly employed.

These features impact the model results presented below, which in many ways are comparable to much finer resolution models. As noted in the introduction, we have chosen not to employ any flux adjustments. The consequences of this approach will also be discussed below.

### 3 Model Results

While differences exist between the atmospheric model used in these experiments and those discussed by Hansen et al. (1983) (see Table 1), nevertheless many of the physical parameterizations are similar. We therefore concentrate on the coupled model results which are functions of the new ocean model or directly impact the results.

#### *a Model dynamical properties and changes with time*

The coupled model was integrated for 120 years, starting with National Meteorological Center atmospheric observations for December 1, 1977, and from the Levitus (1982) ocean climatological temperature and salinity fields at  $1^\circ \times 1^\circ$  resolution interpolated to the model's  $4^\circ \times 5^\circ$  resolution. The marine observed climatology has 33 levels which are vertically integrated to the 13 layers in the ocean model. In the upper 1500 m, a periodic parabolic spline is fit to Levitus' seasonal climatology to obtain values for December 1, when the simulation starts. Below 1500 m Levitus' annual data are used. The column mass of each grid box is solved so that the ocean surface elevation is zero everywhere, i.e. mean sea level. All ocean currents start at zero velocity. The initial height field quickly readjusts to conform to geostrophic flow. The initial heat and salt in the model's straits are calculated by using the ocean values at the two ends of each strait. The initial sea ice distribution for the Northern Hemisphere comes from Walsh and Johnson (1979) and for the Southern Hemisphere from Alexander and Mobley (1976).

To the extent that the observations are representative of actual ocean conditions, the coupled model therefore began its integration with a realistic climatology (which is achieved in other models via the use of flux adjustments or restoring forces). However, if the model results indicated a rapid deterioration away from these initial conditions, to an unrealistic climate state, then it would be relatively useless for climate change experiments without additional measures (such as using flux adjustments). It is therefore important to report how the model dynamics and thermodynamics varied with time. Since the stability of the ocean model dynamics will influence the meaning of the thermodynamic results, we discuss the model dynamical properties first.

Other models use flux adjustments for two different reasons. One is to help generate the thermohaline circulation and related ocean dynamics, and the other is to correct surface energy imbalances which result in climate drift. The first problem is presumably associated with inadequate thermal or hydrologic forcing from the atmosphere, or inadequate dynamical response from the ocean model. The latter effect is associated with a net annual forcing of the surface due, presumably, to deficiencies in the calculations of cloud cover, water vapour, or other important parameters. To assess the adequacy of a model without flux adjustments, both of these issues must be addressed.

For climate purposes, the oceanic poleward transport of heat is of prime importance. Shown in Fig. 2 is the annual ocean heat transport as a function of latitude for years 88–97, compared with observations. (Unless otherwise stated, model re-

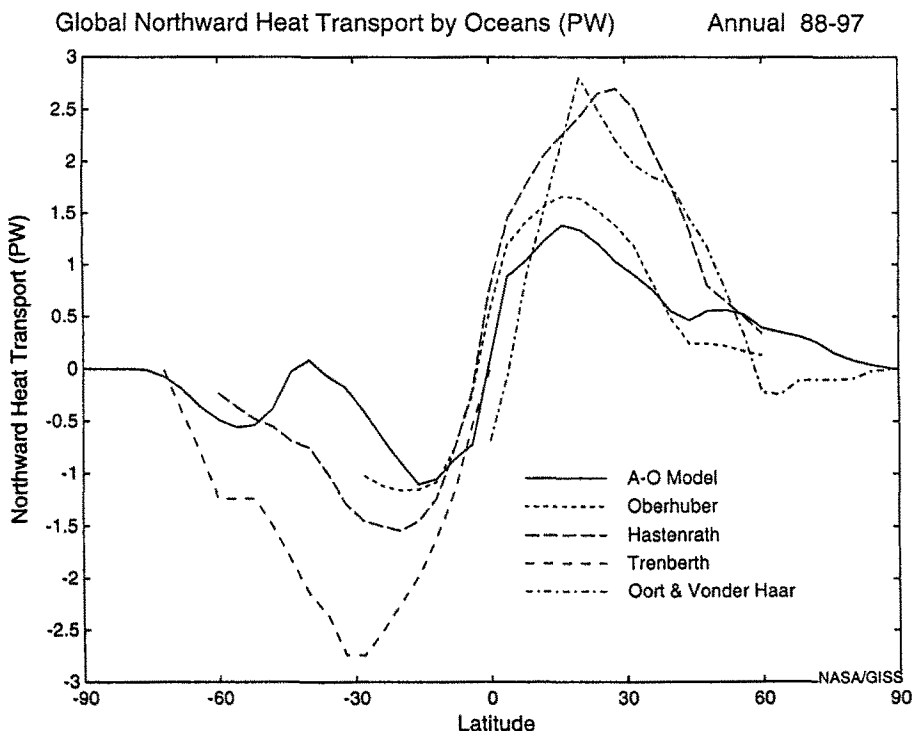


Fig. 2 Global annual northward transport of heat (PW) by the oceans for years 88–97 of the coupled model simulation and observations of Oberhuber (1988); Hastenrath (1980), Trenberth (1979), and Oort and Vonder Haar (1976).

sults are shown for these years as they represent the control run simulation at the time of effective CO<sub>2</sub> doubling in a companion model run with a 1% CO<sub>2</sub> compound increase per year following a 23-year spin-up.) Obviously, the observations contain a wide range of uncertainty; the peak model value of 1.4 PW is about 85% of the Oberhuber value, and some 60% of the peak Hastenrath value. The model magnitude compares favourably to the dynamical ocean heat transports in other coupled atmosphere-ocean models, which are 1.5, 1.3 and 1.2 PW respectively in the Geophysical Fluid Dynamics Laboratory (GFDL) model (Manabe et al., 1991, 1992), the Max-Planck-Institute for Meteorology (MPI) model (Maier-Reimer and Hasselman, 1987), and the U.K. Meteorological Office (UKMO) model (Murphy, 1992). The global maximum transport in the high resolution model of Semtner and Chervin (1992) is 1.4 PW. Thus the GISS model result appears to be similar to that of other models, although all may be somewhat too small.

Washington et al. (1994) noted that one of the major problems in coarse resolution ocean models is that the meridional transport of heat is dominated by subgrid-scale diffusion. Bryan (1987) showed that most GCMs had too little northward heat transport and thermoclines that were too deep. When vertical diffusivities

## Global Annual Northward Heat Transport (PW) at 16°N

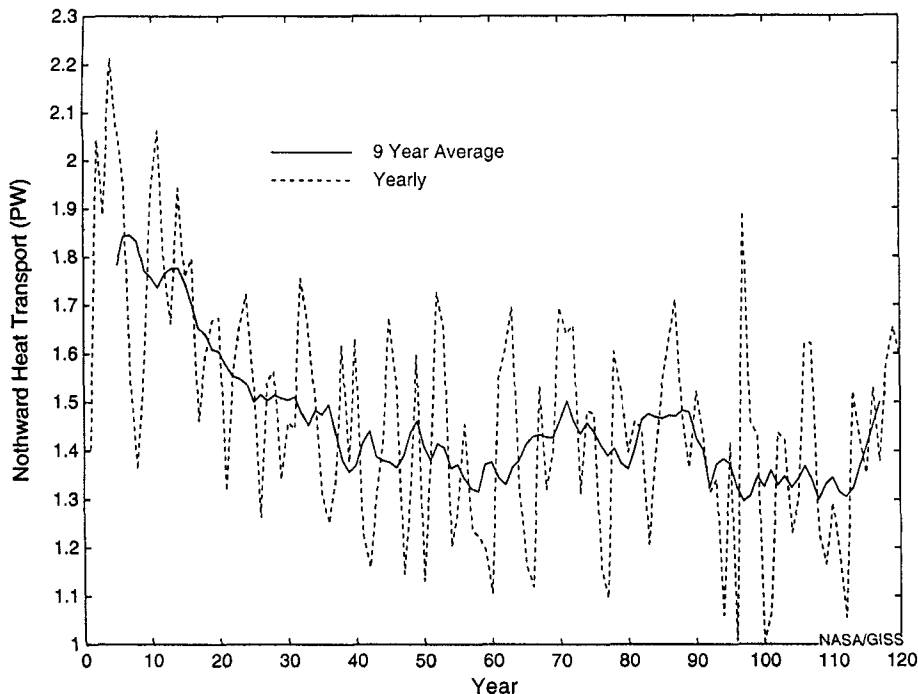


Fig. 3 Global annual northward transport of heat (PW) by the oceans at 16°N for each year of the coupled model simulation.

were reduced, the northward heat transport decreased. The heat transport in the GISS ocean model is higher than in most coupled simulations even though the vertical diffusivity is lower than in most Oceanographic General Circulation Models (OGCMs) (see Table 3). Perhaps since the GISS model uses the linear upstream scheme and does not include horizontal diffusion explicitly, the problems identified by Washington et al. (1994) and Bryan (1987) are not apparent.

How stable is this transport? Shown in Fig. 3 is the temporal variation of the annual northward heat transport at 16°N. During the first 25 years, model values decrease from those associated with the initial conditions by about 25%; subsequently there is little systematic variation over the course of the experiment. The model can apparently sustain its dynamical heat transport sufficiently long to be useful for century-scale transient climate change simulations. Therefore, even without flux adjustments, this aspect of the ocean circulation appears stable in time. Note that the values for years 88–97 for this (and other) diagnostics are representative of the long-term model average.

One of the major difficulties incurred in coupled models without flux adjustments is that the deep water circulation is too weak. That problem is encountered in this model as well. Shown in Fig. 4a is the Atlantic ocean mass stream function for years

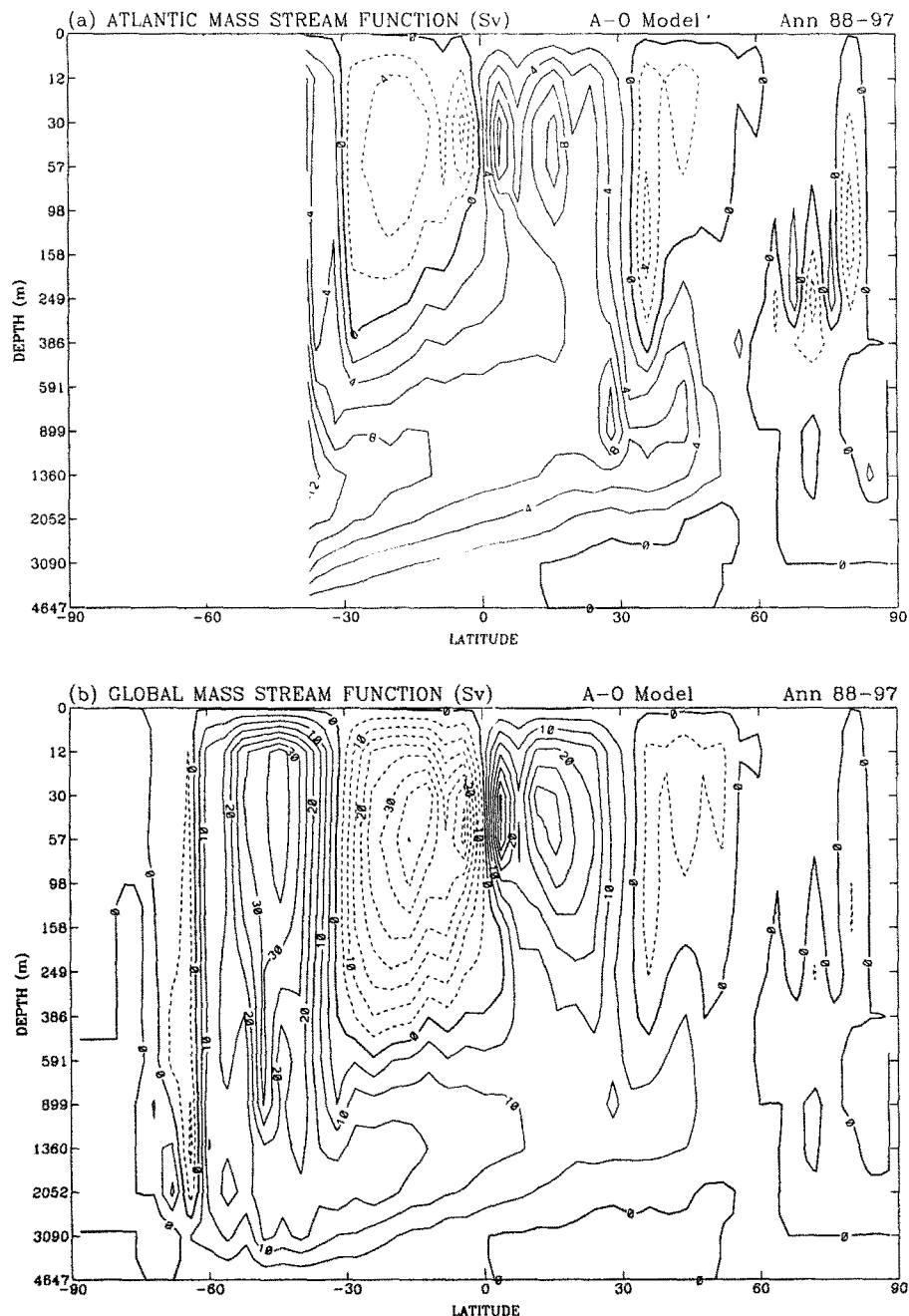


Fig. 4 Annual mass stream function (Sv) for years 88–97 of the coupled model simulation, longitudinally averaged over (a) Atlantic ocean grid boxes, and (b) all ocean grid boxes.

TABLE 7a. Comparison of North Atlantic Stream Function maxima in different models.

PARAMETER	RUSSELL et al.	SEMTNER and CHERVIN (1992)	MANABE et al. (1991)	WASHINGTON et al. (1994)	WASHINGTON and MEEHL (1989).
Type	Coupled	Ocean	Coupled	Ocean	Coupled
Coupled-Model					
Integration (yrs)	120	32.5	100	100	46
Resolution	$4^\circ \times 5^\circ$	$0.5^\circ$	$4.5^\circ \times 7.5^\circ$	$1^\circ$	$5^\circ$
Correction	None	Surface Restoring	Flux Correction	Surface Restoring	None
Magnitude (Sv)	11.2	10	17	9	15
Depth (m)	900	850	1000	1100	50
Latitude	30°N	38°N	37°N	35°N	15°N

TABLE 7b. Comparison of Antarctic Bottom Water global stream function maxima in different coupled models (values are from this paper and estimated from Gates et al., (1993)).

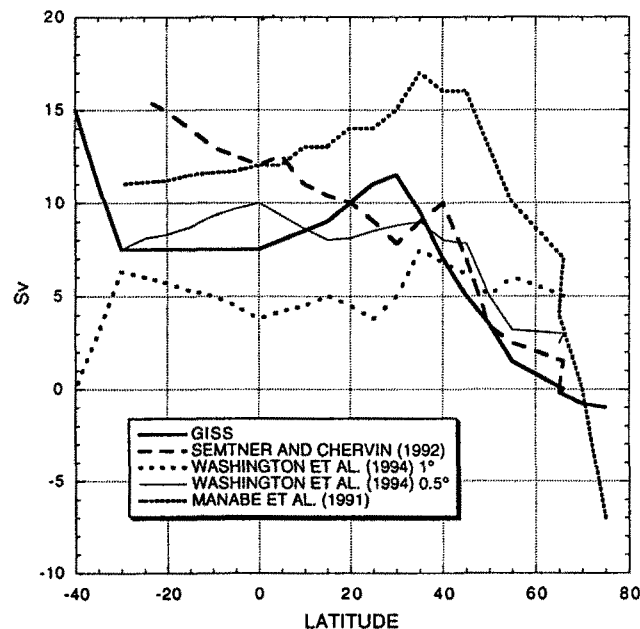
Parameter	GISS	GFDL	MPI	NCAR	UKMO
Resolution	$4^\circ \times 5^\circ$	$4.5^\circ \times 3.75^\circ$	$4^\circ \times 4^\circ$	$5^\circ \times 5^\circ$	$2.5^\circ \times 3.75^\circ$
Correction	None	Flux	Flux	None	Flux
Magnitude (Sv)	12	8	7	6	17
Depth (m)	1100	1900	1700	275	1200
Latitude	65°S	70°S	70°S	65°S	65°S

88-97. The maximum value for the North Atlantic is approximately 11.2 Sv, located at a depth of approximately 900 m at latitude 30°N (note that the vertical coordinate is derived from the model layering). This magnitude represents a decrease of 36% when compared with the first few years of the simulation. Hall and Bryden (1982) indicate that the observed stream function at 25°N and 1150 m is 19.2 Sv, which would imply that the model's value is 40% too small. In addition, during the first 10 years of the simulation the magnitude of the model's stream function was 17.5 Sv at 900 m and 45°N; this has weakened to 6.5 Sv after 100 years.

Shown in Table 7a is a comparison of the North Atlantic mass stream function maxima between these results and those of several other models. This model produces circulations of a similar magnitude to the circulations of much higher resolution ocean models, and at approximately the same depth; however, the maximum occurs further south. The largest value occurs in the Manabe et al. (1991) simulation in which flux adjustments are applied.

Presented in Figs 5a and 5b are the latitudinal and vertical profiles of the Atlantic circulations from the different models, at the depths and latitudes of peak stream function intensity. In both its latitudinal and depth structures, the GISS model has many similarities to the high resolution result of Semtner and Chervin (1992), although, as noted, the GISS model peaks at a lower latitude. A clear increase in

(a) ATLANTIC STREAM FUNCTION AT DEPTH OF MAXIMUM



(b) N. ATLANTIC STREAM FUNCTION AT LATITUDE OF MAXIMUM

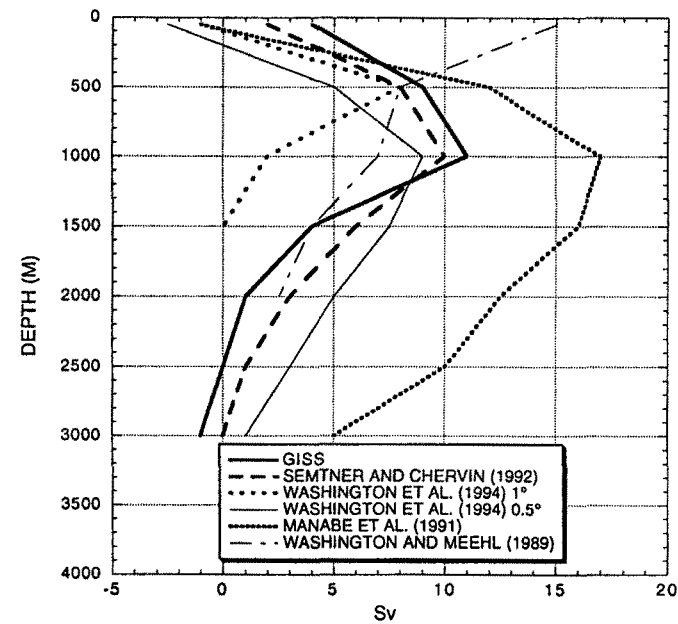


Fig. 5 Annual mass stream function ( $\text{Sv}$ ) for the Atlantic Ocean as a function of (a) latitude and (b) depth at the location where the North Atlantic thermohaline circulation is maximum. See Table 7a.

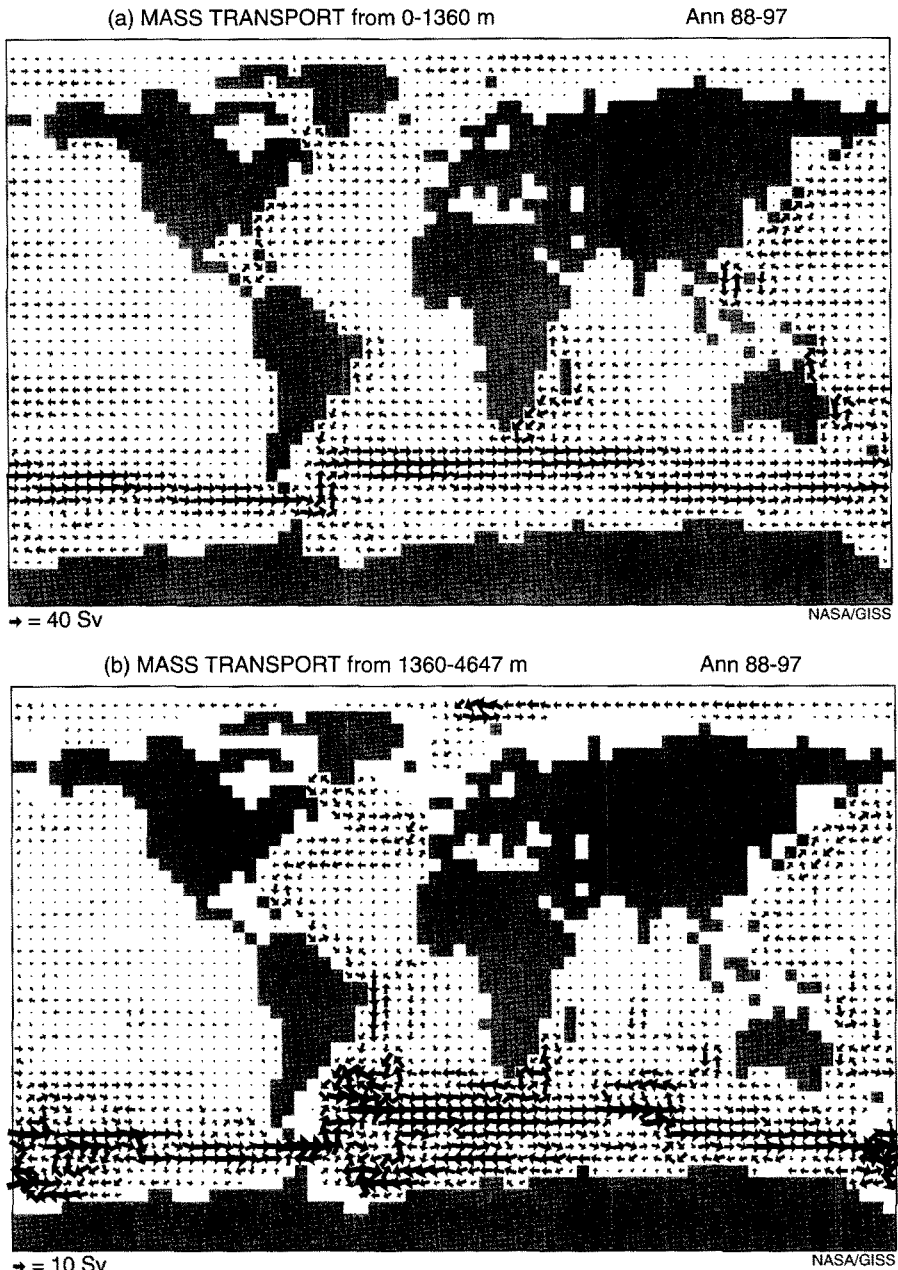


Fig. 6 Annual ocean mass transports, vertically integrated, for years 88–97 of the coupled model simulation for depths (a) 0 – 1360 m; (b) 1360 – 4647 m and (c) 3090 – 4647 m. The area of the arrows are proportional to the flow.

(c) MASS TRANSPORT from 3090-4647 m

Ann 88-97



Fig. 6 Concluded.

intensity is exhibited by the GFDL model; it is perhaps this magnitude of difference which the GISS model misses by not including flux adjustments. England (1993) did a sequence of simulations with a coarse resolution ocean model and found that surface salinity enhancement was especially effective in improving the thermohaline circulation.

The vertical profiles (Fig. 5b) of the circulation cells all have similar shapes, with the one exception being the Washington and Meehl (1989) simulation (which also lacks flux adjustments). In that model the circulation peaks near the surface, and is clearly wind driven. While wind forcing likely is playing a role in the other models as well, at least in the upper 1000 metres, neither higher resolution nor the imposition of flux adjustments changes the vertical profile substantially (although flux adjustments increase its magnitude at most depths).

To examine the structure of deep water formation and flow in more detail, Figs 6(a-c) show the mass transports in the upper ocean above 1360 m (Fig. 6a), in the deep ocean from 1360 m to 4647 m (Fig. 6b), and in the lowest level from 3090 to 4647 m (Fig. 6c). North Atlantic Deep Water (NADW) formation is occurring in the Labrador Sea, and in the vicinity of the Greenland-Iceland-Norwegian Sea. (Note that because of the vertical and horizontal resolution, the Denmark strait is blocked at 386 m, and the passage between Iceland and northern Europe is blocked below 899 m (Fig. 1)). It then flows south along the western boundary of the ocean to the vicinity of the Antarctic Circumpolar Current. The first few years of the simulation,

which should be closer to reality, and the high resolution model results of Semtner and Chervin (1992) both show a very similar pattern to that in Fig. 6b, except that the Labrador Sea flow should be moving southward in the region to the west of the mid-Atlantic Ridge. In addition, during the first few years, the Labrador Sea component was substantially stronger. This is consistent with the weakening of the northern portion of the Atlantic stream function diagnostic during the course of the model simulation.

The "conveyor belt" in the model continues with NADW flowing eastward south of Africa, through the southern Indian Ocean, turning northward east of Australia and meandering weakly into the North Pacific, primarily in the western portion of the basin. The results were similar during the first few years, except the northward flow was located more towards the centre of the North Pacific. In the Semtner and Chervin (1992) reconstruction, the western portion seemed to be favoured.

Fig. 4b shows the latitude-depth distribution of the annual stream function averaged over all the world's oceans. Table 7b shows that the peak Southern Hemisphere circulation cell associated with Antarctic Bottom Water (AABW) production is similar to other coupled models. Note that without flux adjustments and with only four layers, the NCAR model lacks the ability to produce a deep circulation cell at high latitudes in the Southern Hemisphere (Gates et al., 1993).

However, Fig. 4b also indicates the lack of zonally averaged circulation which would allow the AABW to be transported north of the circumpolar current (and would appear as a negative circulation cell at mid-latitudes in the Southern Hemisphere in the lower layers). Reference to Fig. 6c, indicating the deepest water circulation, shows that AABW is in fact being generated in the Weddell and Ross seas and moving equatorward, primarily in the South Atlantic. In the vicinity of the equator it encounters the mid-Atlantic ridges (thus the model level disappears) and the flow continues across the equator at a shallower depth (Fig. 6b). This result is again similar to that of the first few years, although somewhat weaker. The high resolution model results of Semtner and Chervin (1992) are less coherent about this feature, probably because of their ability to generate high resolution eddies. (The lack of a negative circulation cell at mid-latitudes in the Southern Hemisphere on the zonal average in Fig. 4b appears to be due to the large poleward flow in the vicinity of 30°W, as well as reduced equatorward flow from the Ross Sea, compared with the first few years.)

How are the model dynamical circulations varying with time? In Fig. 7 we show the vertically-integrated equatorward flow at 32°N at the longitudes of peak mass transport and at 64°S integrated over all longitudes. The North Atlantic equatorward flow in this region is relatively stable. The Antarctic Bottom Water return flow undergoes oscillations, with the values after 120 years being as large or larger than at the beginning of the experiment.

However, this integrated value does not imply that changes are not occurring even at these longitudes. In the Northern Hemisphere the peak equatorward transport, which initially was almost entirely at a depth of 900–1000 m, is gradually

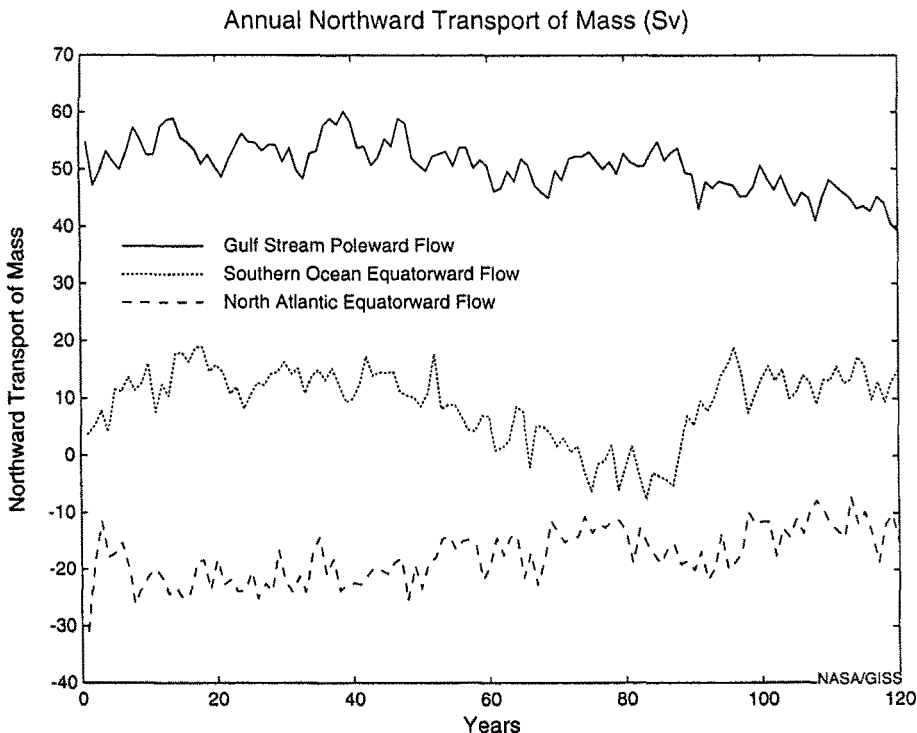


Fig. 7 Annual northward transport of mass for each year of the coupled model simulation for the Gulf Stream poleward flow at  $32^{\circ}\text{N}$  (coastal grid boxes down to 2052 m), the southern ocean bottom water equatorward flow at  $64^{\circ}\text{S}$  (flow at all longitudes from 899 m to the bottom) and North Atlantic equatorward flow at  $32^{\circ}\text{N}$  (two grid boxes from  $75^{\circ}\text{W}$  to  $65^{\circ}\text{W}$  except for the two layers that intersect the Gulf Stream).

becoming less concentrated, and extending to shallower levels. The phenomenon is associated with a reduction in the depth of convection in sea ice regions. As will be discussed below, one consequence of the model's slow climate drift, and the simple sea ice parameterization being employed, is that sea ice is diminishing in some regions of the North Atlantic. Sea ice formation increases the density and convective instability, so one result of the sea ice tendency is a gradual shallowing of the thermohaline circulation. In the Southern Hemisphere, the Antarctic Bottom Water circulation is also being affected by sea ice changes, as well as by melting from the Antarctic continent. Sea ice variations with time will be discussed in Section 3b.

Maintenance of the thermohaline circulation is important for maintaining the separation between the upper and deep ocean spheres. One problem which has historically existed in models without flux adjustments is the inability to preserve the thermocline structure. We show in Fig. 8 (a-d) the potential temperature, salinity

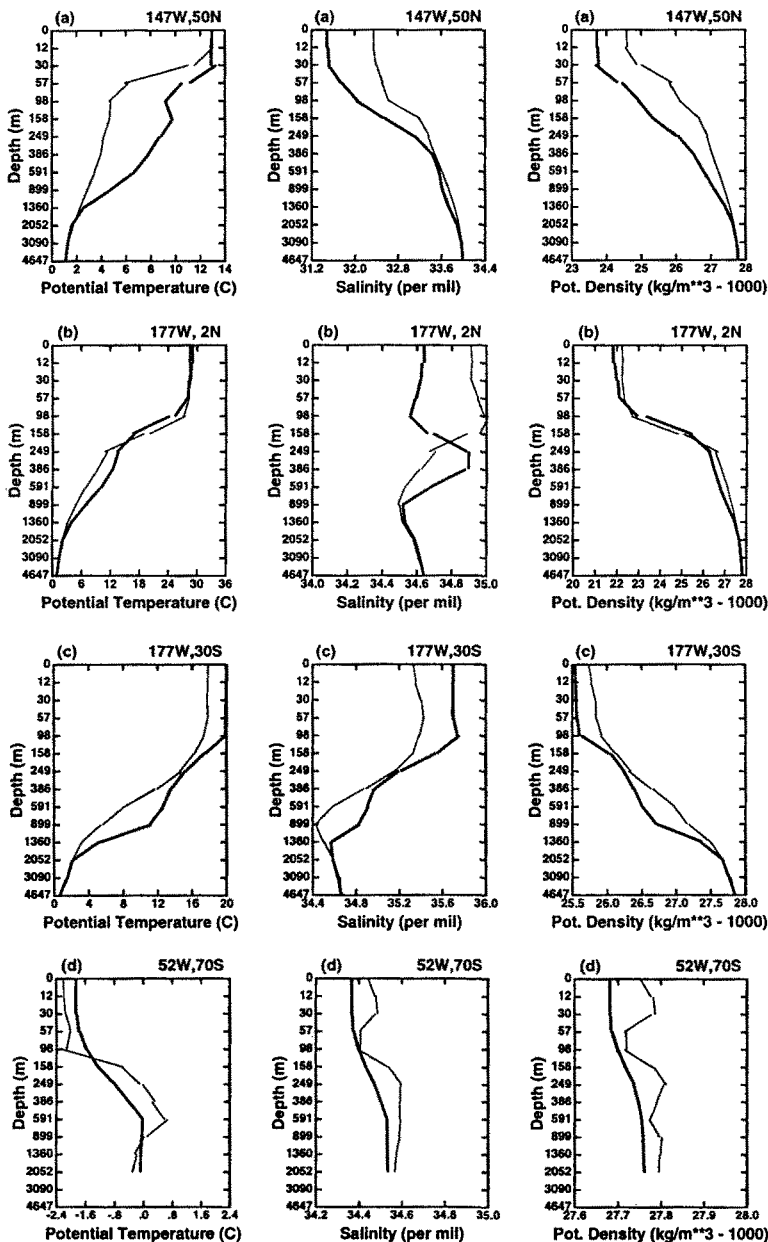


Fig. 8 Depth profiles of potential temperature ( $^{\circ}\text{C}$ ), salinity (per mil) and potential density ( $\text{kg}/\text{m}^3 - 1000$ ) on September 1 for the coupled model simulation on year 93 (thick line) and for the observations of Levitus (1982) (thin line) for four locations (a)  $147^{\circ}\text{W}$ ,  $50^{\circ}\text{N}$  near ocean station Papa; (b)  $177^{\circ}\text{W}$ ,  $2^{\circ}\text{N}$ ; (c)  $177^{\circ}\text{W}$ ,  $30^{\circ}\text{S}$  and (d)  $52^{\circ}\text{W}$ ,  $70^{\circ}\text{S}$  in the Weddell Sea.

and potential density profiles at northern and southern latitudes, for an arbitrary day (September 1) in the Levitus initial conditions and 93 years into the run. In general, the model has preserved the structure of the seasonal and permanent thermocline over a range of latitudes; even in the Weddell Sea, which is characterized by extremely small gradients, there has been only a slight smoothing. The accuracy of the linear upstream scheme for heat and moisture advection, and the related limited diffusion used in this model, undoubtedly help in the maintenance of vertical gradients. There is a tendency for some warming to have occurred at mid-depths associated with the model's climate drift, as discussed in Section 3b below.

The vertically integrated horizontal mass transports above 1360 m are shown in Fig. 6a. The major anticyclonic gyres and the Antarctic Circumpolar Current are well represented. The intensification of currents along the western boundaries is also apparent in the northern oceans and somewhat weaker in the southern oceans. There are generally strong currents in the opposite direction near the western boundary current, in conformity with observations.

Among the world's major currents are the Kuroshio Current, the Gulf Stream and the Antarctic Circumpolar Current (ACC). For the Kuroshio Current, the model's annual northward mass transport is 70 Sv across 32°N at 138°E. For the Kuroshio Extension at 165°E, Joyce and Schmitz (1988) found a total eastward transport of 57 Sv at 34°N and westward transport to the north and south. For the Gulf Stream across 32°N at 77°W, the northward transport is approximately 48 Sv. Halkin and Rossby (1985) calculated a transport of 88 Sv based on temperature and velocity sections at 36°N, 73°W. In both the Kuroshio and Gulf Stream systems, the model produces strong southward transports in the two adjacent grid boxes to the east.

The model's mean transport through the Drake Passage is 146 Sv. Nowlin and Klinck (1986) observed a mean of 134 Sv and Whitworth (1983) obtained 123 Sv using a year-long monitoring array and hydrographic data. Whitworth and Peterson (1985) found that most of the transport is in the baroclinic field and most of the variability is in the barotropic field. They also found that the magnitude of the transport varied seasonally with the minimum transport occurring in July. The coupled model shows a minimum transport of 137 Sv through the Drake Passage in September.

How do the mass transports of the major current systems change with time? The variation of the Gulf Stream transport is shown in Fig. 7. Again it has remained relatively stable, although there has been a slight decrease with time as well as a shift to deeper levels (associated with the gradual shallowing of the NADW return flow). The relative constancy of this and other circulation features leads to the relative stability of the peak heat transports (Fig. 3). During the course of the model simulation, the flow through the Drake passage varied from a peak of 160 Sv at the beginning, to 125 Sv around year 60; by year 120, the value was back up to 158 Sv.

One of the novel features of the present ocean model is that it does not use the "rigid-lid approximation". Instead, it conserves mass, allows divergent flow and

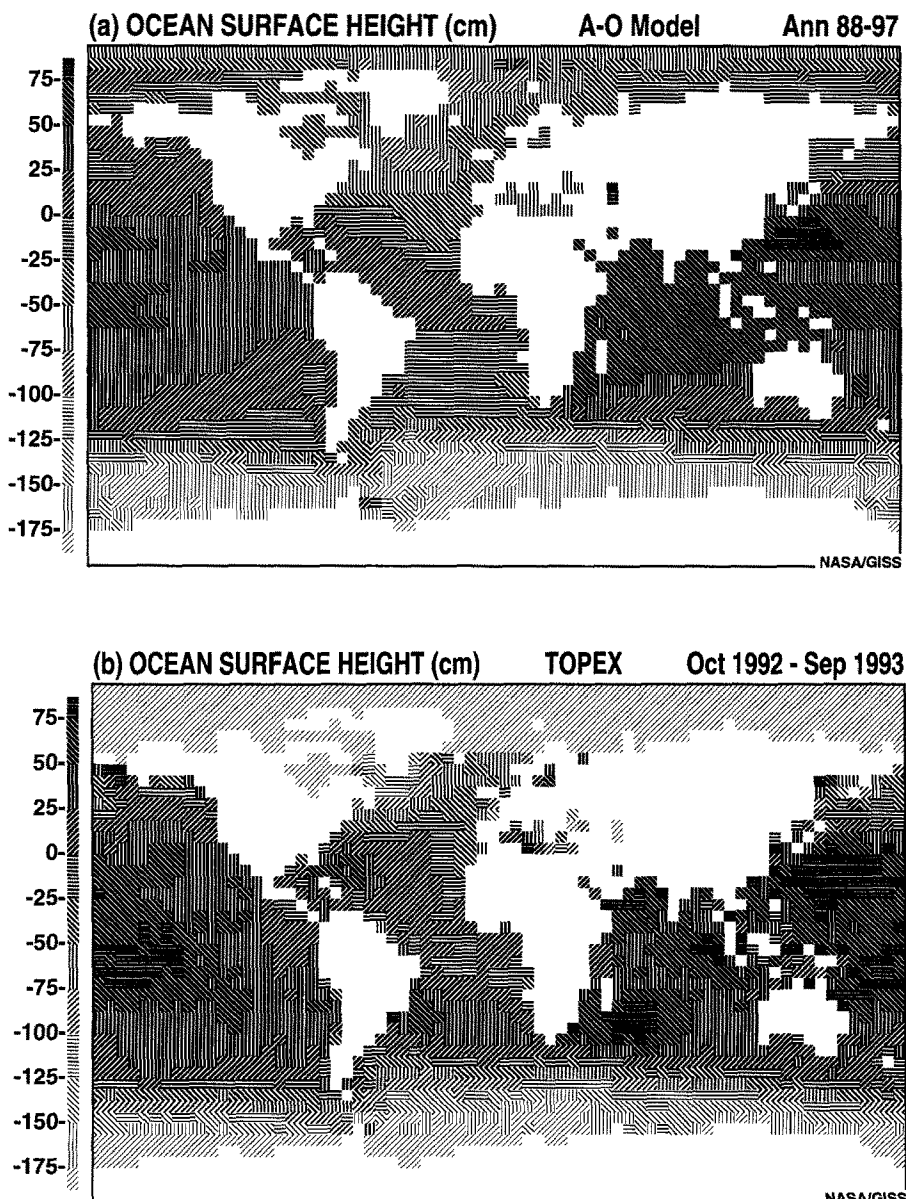


Fig. 9 Annual ocean surface height (cm) for (a) years 88–97 of the coupled model simulation and (b) observations of TOPEX (Callahan, 1993; Stammer and Wunsch, 1994). The TOPEX data is defined only between 70°S and 70°N. Model values have been raised by 66.32 cm because the global sea level has sunk by that amount.

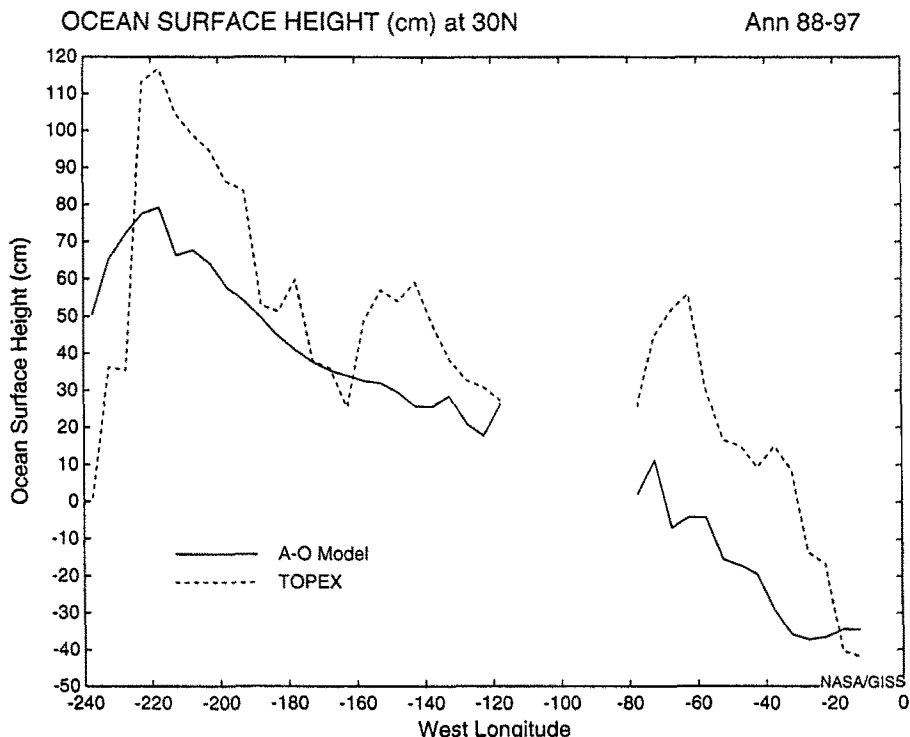


Fig. 10 Annual ocean surface height (cm) across  $30^{\circ}\text{N}$  for years 88–97 of the coupled model simulation and the observations of TOPEX (Callahan, 1993; Stammer and Wunsch, 1994). Model values have been raised by 66.32 cm because the global sea level has sunk by that amount.

calculates the ocean surface height field directly. The free surface would allow tides to be predicted and tsunamis to be propagated by the ocean model. Fig. 9 shows the annual ocean surface height for years 88–97 of the coupled model simulation and the Ocean Topography Experiment (TOPEX) observations for one year (Callahan, 1993; Stammer and Wunsch, 1994). The height fields show the major anticyclonic gyres in the Atlantic and Pacific Oceans.

Fig. 9 has been corrected for a systematic difference between the coupled model and the TOPEX observations due to global changes in sea level which arose during the course of the model integration. At the beginning of the model simulation the global ocean surface height was zero, consistent with TOPEX, whereas by years 88–97 of the integration the global ocean height is 66 cm lower. During those 97 years, snow has accumulated on the northern hemisphere ice caps and on Antarctica, as will be discussed below.

In both the Pacific and Atlantic basins, the surface height decreases toward the east. Fig. 10 shows the annual height field across  $30^{\circ}\text{N}$  in the Pacific for the coupled model (corrected for the global sea level change) and the TOPEX observations. The

TABLE 8. Annual eastward transport of mass ( $10^8$  kg/s) as a function of latitude and layer depth (m) along the International Date Line for years 88–97 of the coupled model simulation.

Lat	Sum	6	21	44	77	128	204	318	489	745	1129	1706	2571	3868
62°N	-10	-6	-2	-2	-1	1	0	0	0	0	0	0	-	-
58°N	24	4	1	0	0	-3	-3	-3	-1	7	11	11	0	-
54°N	-140	-1	-3	-4	-5	-6	-9	-14	-19	-27	-29	-20	-1	0
50°N	43	4	0	-1	-2	-2	-1	1	4	8	10	10	9	2
46°N	197	5	3	5	9	14	19	25	31	34	32	21	7	-8
42°N	100	6	4	5	9	13	17	21	20	13	2	-5	-5	1
38°N	28	4	3	5	6	9	11	12	7	-2	-11	-15	-11	10
34°N	12	1	1	1	2	2	4	6	8	3	-4	-7	-5	-1
30°N	-36	0	2	2	2	0	-4	-7	-10	-13	-10	-2	4	0
26°N	-117	0	4	3	2	-3	-14	-31	-43	-35	-13	5	9	0
22°N	-153	-7	-3	-7	-12	-19	-28	-34	-31	-15	4	8	-1	-8
18°N	-88	-11	-9	-15	-22	-25	-21	-9	7	17	12	-3	-9	0
14°N	-12	-7	-3	-6	-5	-3	-4	2	12	13	-2	-11	-3	6
10°N	47	8	17	23	20	2	-4	1	1	-5	-10	-5	2	-4
6°N	92	5	12	16	19	17	20	15	3	-3	-5	0	-2	-6
2°N	43	-36	-41	-37	2	81	63	19	1	2	-2	-1	-9	2
2°S	-5	-35	-40	-39	-7	67	54	14	-3	-5	-4	4	-7	-4
6°S	103	7	13	17	14	7	15	22	13	-3	-3	1	-3	2
10°S	156	9	18	24	26	15	12	22	23	11	-3	-8	-9	15
14°S	-17	-6	-3	-5	-4	1	-3	-6	-1	5	4	0	0	0
18°S	-174	-9	-7	-13	-21	-30	-35	-36	-27	-14	10	7	0	0
22°S	-186	-4	-1	-4	-9	-15	-24	-32	-40	-39	-22	4	0	0
26°S	-170	-2	2	2	0	-4	-12	-27	-46	-62	-51	-12	42	0
30°S	-233	-1	0	-1	-4	-8	-15	-25	-38	-45	-36	-30	-31	0
34°S	101	0	0	0	1	2	2	0	0	-1	3	47	47	0
38°S	-37	5	1	0	-1	-2	-2	-3	-5	-3	-28	0	0	0
42°S	22	-2	-2	-2	-1	0	1	1	1	-19	44	0	0	0
46°S	601	14	13	20	29	41	59	83	104	117	114	8	0	0
50°S	462	11	12	18	27	39	55	72	87	94	40	8	0	0
54°S	380	7	3	4	5	7	10	15	22	25	50	76	80	76
58°S	341	4	5	7	11	17	25	34	44	54	51	49	29	9
62°S	95	6	4	5	7	10	14	20	27	33	31	4	-36	-30
66°S	-373	-6	-3	-5	-7	-10	-14	-22	-32	-48	-60	-68	-99	0
70°S	259	1	2	3	5	7	10	15	21	34	40	39	82	-
74°S	-19	-12	-1	-2	-1	-1	-1	-1	0	-	-	-	-	-
78°S	12	2	2	2	2	2	2	1	-1	-	-	-	-	-

coupled model shows a range of 61 cm across the Pacific Ocean from 220°W to the Mexican coast whereas the TOPEX observations show a range of 99 cm. Tau (1988) has made direct estimates of absolute dynamic topography from satellite altimetry, and showed a 75 cm maximum above mean sea level in the North Pacific gyre. This compares favourably with the model result (at longitude -220°), but is less than the TOPEX observation. A surface height decrease also occurs toward the south across the Antarctic Circumpolar Current (Fig. 9). Peterson (1988) showed that the annual cycle in wind stress curl influences the sea level rise across the entire Antarctic Circumpolar Current.

Table 8 shows the meridional-depth cross section of eastward mass transport at the International Dateline. The model resolves the surface equatorial countercurrent

TABLE 9. Annual transport of conserved quantities through the 12 straits of the coupled model for years 88–97 as a function of layer depth (m).

	Sum	6	21	44	77	128	204
<i>Transport of Mass (<math>10^6</math> kg/s)</i>							
Fury & Hecla	109	56	52	—	—	—	—
Nares	-11233	-1918	-2400	-2314	-2483	-2119	—
Gibraltar	71	295	345	215	-486	-299	—
English	1	-16	16	—	—	—	—
Kattegat	-22	-110	89	—	—	—	—
Bosphorus	0	-15	14	—	—	—	—
Red Sea	-20	-751	-777	-504	88	1993	-69
Bab-al-Mandab	-34	-269	-341	-292	54	897	-83
Hormuz	-16	-118	102	—	—	—	—
Malacca	-169	-79	-60	-30	—	—	—
Korea	1129	751	720	175	-517	—	—
Soya-kaikyo	1127	766	361	—	—	—	—
<i>Transport of Heat (<math>10^{11}</math> W)</i>							
Fury & Hecla	-4	-2	-2	—	—	—	—
Nares	281	60	64	55	56	46	—
Gibraltar	147	261	287	168	-365	-204	—
English	-4	-11	6	—	—	—	—
Kattegat	-6	-37	32	—	—	—	—
Bosphorus	4	-8	12	—	—	—	—
Red Sea	-103	-947	-947	-607	113	2354	-69
Bab-al-Mandab	-68	-347	-428	-352	68	1052	-61
Hormuz	-23	-146	123	—	—	—	—
Malacca	-221	-102	-79	-39	—	—	—
Korea	1130	713	630	128	-341	—	—
Soya-kaikyo	732	508	224	—	—	—	—
<i>Transport of Salt (<math>10^5</math> kg/s)</i>							
Fury & Hecla	36	19	17	—	—	—	—
Nares	-3766	-642	-804	-776	-833	-711	—
Gibraltar	12	108	126	79	-184	-116	—
English	1	-5	6	—	—	—	—
Kattegat	0	-24	24	—	—	—	—
Bosphorus	4	-2	6	—	—	—	—
Red Sea	0	-275	-284	-185	32	736	-25
Bab-al-Mandab	0	-96	-122	-104	20	331	-29
Hormuz	0	-44	44	—	—	—	—
Malacca	-51	-24	-18	-9	—	—	—
Korea	386	257	247	60	-177	—	—
Soya-kaikyo	385	262	124	—	—	—	—

and the equatorial undercurrent at the equator. It shows a net mass transport between  $4^\circ\text{N}$  and  $4^\circ\text{S}$  of 29.8 Sv at depths of 100–400 m. A finer resolution ocean model would likely improve the representation of current systems in the equatorial region.

The coupled model calculates the transports of mass, heat and salt through 12 ocean straits (Table 4). Given in Table 9 are the annual transports of conserved quantities. While these transports are important for realistic simulations in certain

regions, the excessive flow through the Nares strait may reduce the southward large-scale flow east of Greenland.

### **b Model thermodynamic/climatic properties and climate drift**

The other major function for which flux adjustments are used is to remove climate drift. A primary reason for this is the inaccurate energy forcing of the ocean surface due to inadequacies of the atmospheric model (i.e., cloud cover, evaporation, etc.). The atmospheric model used for this simulation had an annual imbalance of  $7.4 \text{ W m}^{-2}$  into the global ocean surface. This is similar to the magnitude of the imbalance in the simulations of Hansen et al. (1984), in which excess solar radiation was removed at the ocean surface, i.e., a flux correction was applied. (Alternatively, changes in the solar constant are sometimes used.) The coupled model had a net imbalance of  $3.7 \text{ W m}^{-2}$  into the ocean at the end of its 120-year integration.

One effect of this imbalance is given in Fig. 11, which indicates that the ocean temperature is increasing at all depths. The global annual warming, mass weighted over all ocean depths, is  $0.007^\circ\text{C year}^{-1}$ . However, different levels warm at different rates. For example, the sea surface and the first 12 m, which can warm and radiate energy outward, undergo a temperature change of  $1.2^\circ\text{C}$  during the first 25 years, after which there is a very small climate drift ( $<0.002^\circ\text{C year}^{-1}$ ). The deeper layers warm continually, with the peak warming occurring at depths between 400 and 900 m; apparently vertical mixing is sequestering the additional heat to this depth with maximum efficiency. In contrast, the lowest layers (with the largest heat capacity) are warming very little.

This ocean climate drift compares favourably with that of Washington and Meehl (1989): over the first 50 m, the GISS model's temperature increase is  $0.014^\circ\text{C year}^{-1}$  compared to  $0.02^\circ\text{C year}^{-1}$  for the NCAR model; at 450 m,  $0.02^\circ\text{C year}^{-1}$  compared with  $0.05^\circ\text{C year}^{-1}$ ; at 1000 m,  $0.015^\circ\text{C year}^{-1}$  compared with  $0.03^\circ\text{C year}^{-1}$ , and in the lowest layer,  $0.002^\circ\text{C year}^{-1}$  compared with  $0.005^\circ\text{C year}^{-1}$ . Note that the National Center for Atmospheric Research (NCAR) model's maximum climate drift occurs at a similar depth to the GISS model, and that the NCAR model also does not use flux adjustments to alleviate this problem.

Is the coupled model climate drift, including values over land, unacceptably large? The answer depends upon the problem being considered. Over the 75-year time span of the IPCC experiments (starting from year 24 of the coupled model simulation), the global surface air temperature in the control run warms by less than  $0.5^\circ\text{C}$  (hence a climate drift of  $\sim 0.006^\circ\text{C year}^{-1}$ ), while the 1% CO<sub>2</sub> compound increase experiment warms by  $1.4^\circ\text{C}$  relative to the control run (hence  $1.9^\circ\text{C}$  overall). For this magnitude of change it may be argued that the climate drift is within acceptable limits; the Washington and Meehl model has been used for numerous future transient climate change studies (e.g. Washington and Meehl, 1989; Meehl, 1990; Meehl et al., 1993a,b; Meehl and Washington, 1993; Washington et al., 1994). On the other hand, the global warming estimated from 1850 to 1990 is on the order of  $0.5^\circ\text{C}$ ; for simulations of this time period, the climate drift is

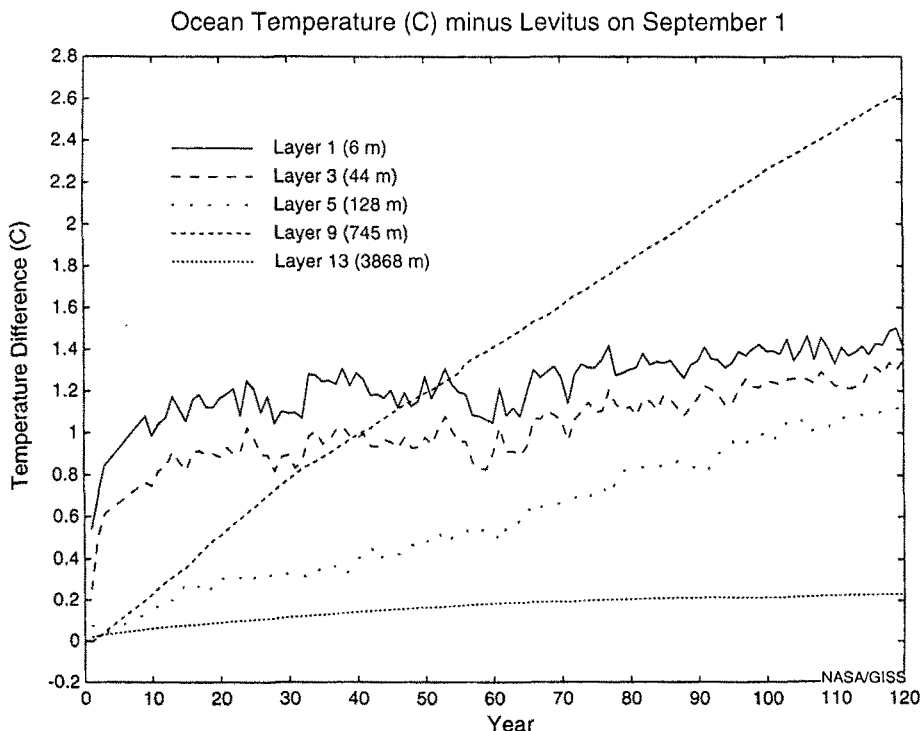


Fig. 11 Temperature change ( $^{\circ}\text{C}$ ) from Levitus (1982) conditions on September 1 for different globally averaged model layers for each year of the coupled model simulation.

probably too large. In terms of its effect on the model itself, the results from the previous section did not indicate any catastrophic dynamical changes as a function of time associated with this drift, although a slow shallowing of the NADW return flow does occur.

One possibility for the annual flux imbalance may be a poor specification of the ocean surface albedo, which comes from spectral reflectance considerations (Hansen et al., 1983). The ISCCP data (Zhang et al., 1995; Rossow and Zhang, 1995) show a global surface albedo over the open ocean of about 8% whereas the model has an albedo of about 5%. The ERBE data also shows ocean albedos to be higher than expected from theory (Barker et al., 1994). A 3% reduction of surface albedo corresponds to about  $6 \text{ W m}^{-2}$  of solar energy added to the ocean, which is much of the atmospheric model's imbalance.

A comparison between the ocean surface temperature for years 88–97 and the observed data from Levitus (1982) is given in Fig. 12. The primary deficiencies occur along the west coast of the continents. The root mean-square error of the sea surface temperatures, compared with the values of Levitus (1982) or Robinson and

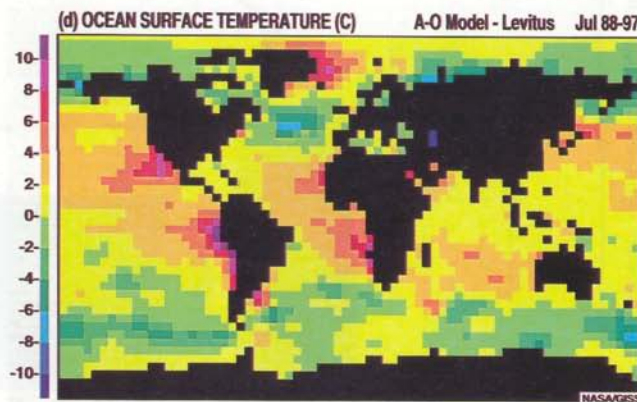
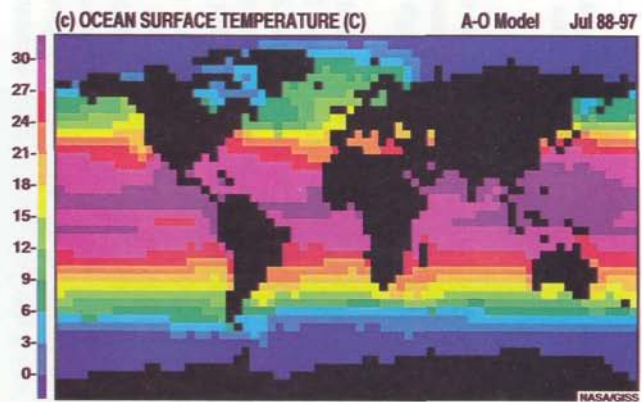
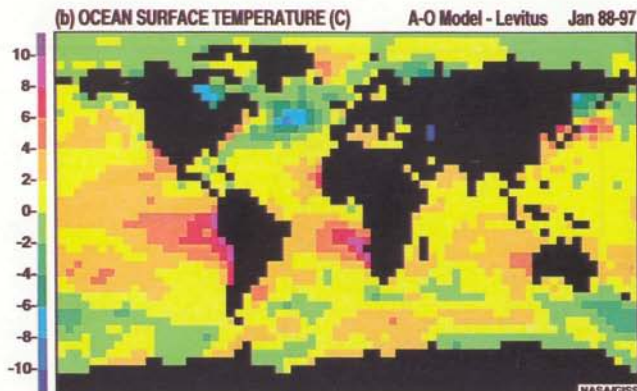
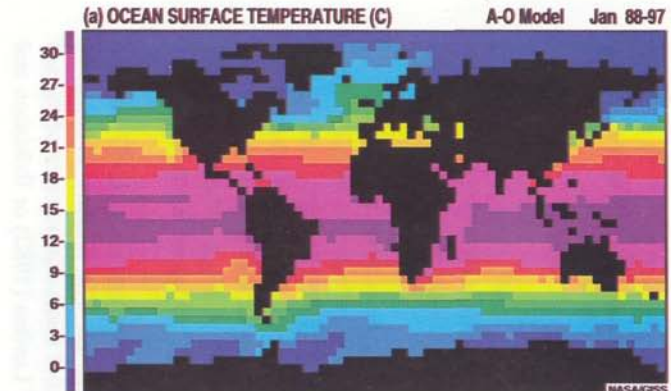


Fig. 12 Ocean surface temperature ( $^{\circ}\text{C}$ ) for (a) years 88–97 of the coupled model simulation for January; (b) the coupled model simulation minus observations of Levitus (1982) for January; (c) the coupled model simulation for July and (d) the coupled model simulation minus observations of Levitus for July. The Levitus temperatures were not defined over the Black Sea, Caspian Sea, nor two northern inlets.

Bauer (1982) is about 2.5°C; the global mean sea surface temperature at this time is 19.2°C compared with the observed value of 18.2°C.

As indicated by this last comparison, the sea surface temperature is too warm globally due to the climate drift (most of which occurs during the first 25 years). Solar radiation is the primary source of heat to the global ocean. Compared with the observations of Bishop and Rossow (1991), on the global average the model values are in agreement (e.g. about 0.3%, or 0.5 W m<sup>-2</sup> different). However, given in Fig. 13 is the incident solar radiation at the ocean surface for the coupled model compared with the observations of Bishop and Rossow (1991). Comparison with Fig. 12 shows that some of the regions which are too warm, primarily those located off the west coasts of continents, also receive too much solar radiation. These regions have too few clouds and the solar radiation reaching the surface is undoubtedly contributing to some of the excess warmth. However, in the atmospheric model these regions do have more cloud cover; it is the coupled system which is losing the clouds.

Ultimately, the absolute global ocean surface temperature is determined by the heat flux at the ocean surface and dynamical interactions with lower levels. The model's annual average surface heat fluxes (the sum of net radiation, latent, sensible and precipitation heat fluxes) are compared with the observations of Esbensen and Kushnir (1981) in Fig. 14. The overall pattern of gain at low latitudes and loss at high latitudes is simulated, although the model has some mid-latitude regions of ocean heat input. In a few locations, such as in the tropical Pacific and eastern subtropical Atlantic, excess heat input is associated with the warmer-than-observed sea surface temperatures (Fig. 12). In other locations (eastern subtropical Pacific, eastern tropical Atlantic) the relationship is reversed, as the excessively warm sea surface temperatures are associated with too little heat input; apparently, in these cases, the warm temperatures result in too much latent heat loss.

In the tropical locations, the excess heat input is due to a reduction in low-level clouds. The atmospheric model, when run with the observed specified ocean temperatures produces low clouds over the cool tropical waters in approximate agreement with observations. When the cold ocean waters start warming up (anomalously), low-level clouds dissipate, allowing more solar radiation to reach the surface. The positive feedback then amplifies the original discrepancy.

The origin of the warm temperatures along the west coasts of continents is likely associated with weak wind stresses in these areas. Shown in Fig. 15a are the model wind stresses, which can be compared with observed values from Hellerman and Rosenstein (1983) (Fig. 15b). Stronger wind stresses would drive greater upwelling, bringing colder water to the surface. The atmospheric model's relatively coarse grid underestimates the topography on the western sides of continents, which may contribute to the weaker winds in these regions.

Smaller scale vertical mixing processes may also play a role. The vertical diffusion coefficients at 30 m for the extreme seasons are shown in Fig. 16. As noted in Table 3, the GISS model has weaker vertical diffusion than some other models.

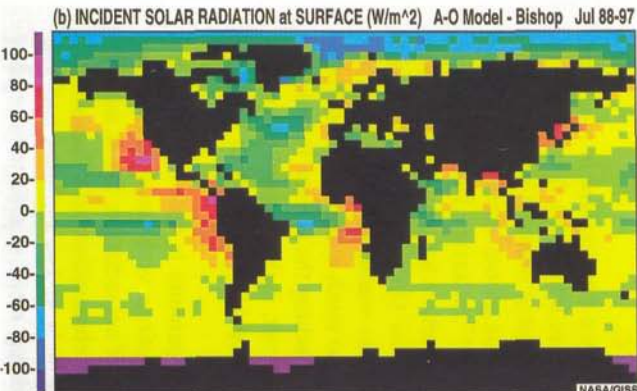
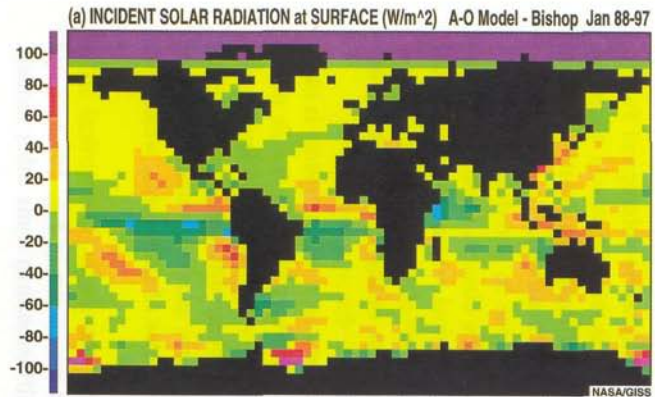


Fig. 13 Incident solar radiation at the surface (W/m<sup>2</sup>) for years 88–97 of the coupled model simulation minus the observations of Bishop and Rossow (1991) for (a) January and (b) July.

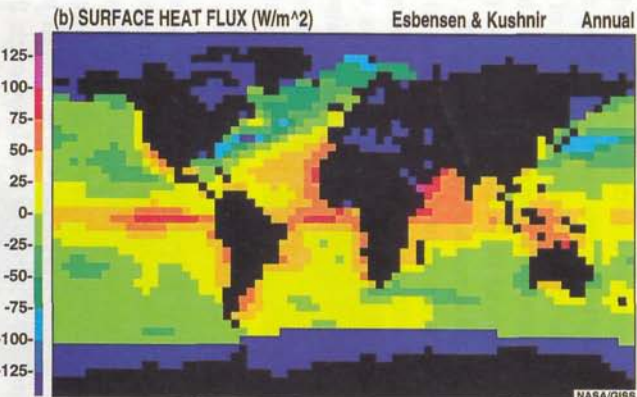
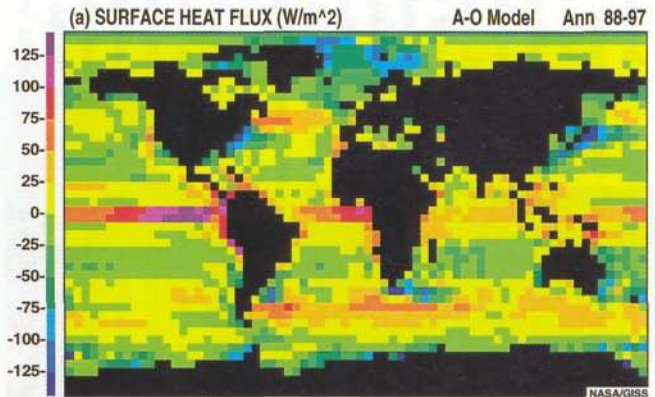


Fig. 14 Annual surface heat flux (W/m<sup>2</sup>) for (a) years 88–97 of the coupled model simulation and (b) observations of Esbensen and Kushnir (1981). The observed heat flux was not defined over sea-ice.

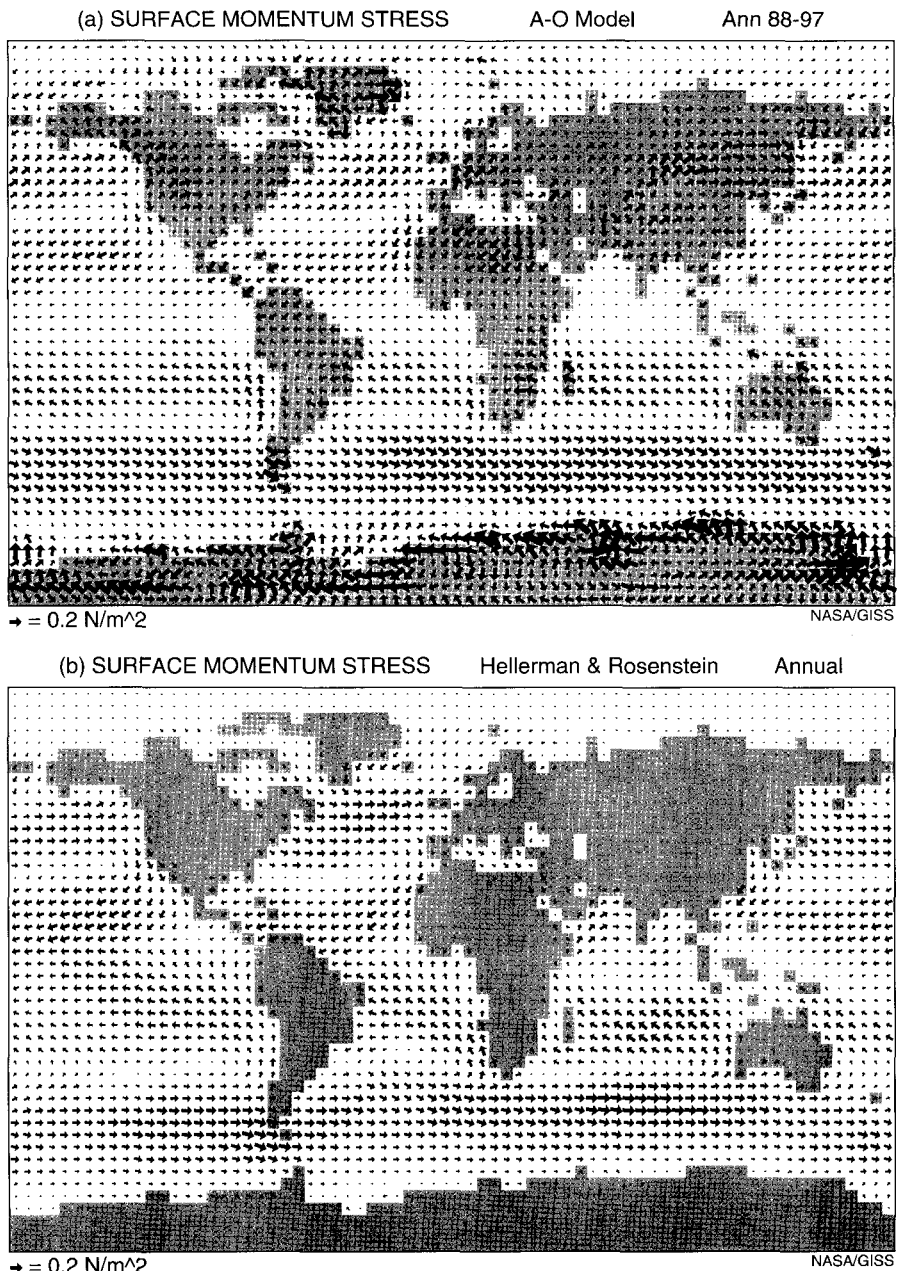


Fig. 15 Annual surface momentum stress for (a) years 88–97 of the coupled model simulation and (b) observations of Hellerman and Rosenstein (1983). The area of the arrows are proportional to the stress.

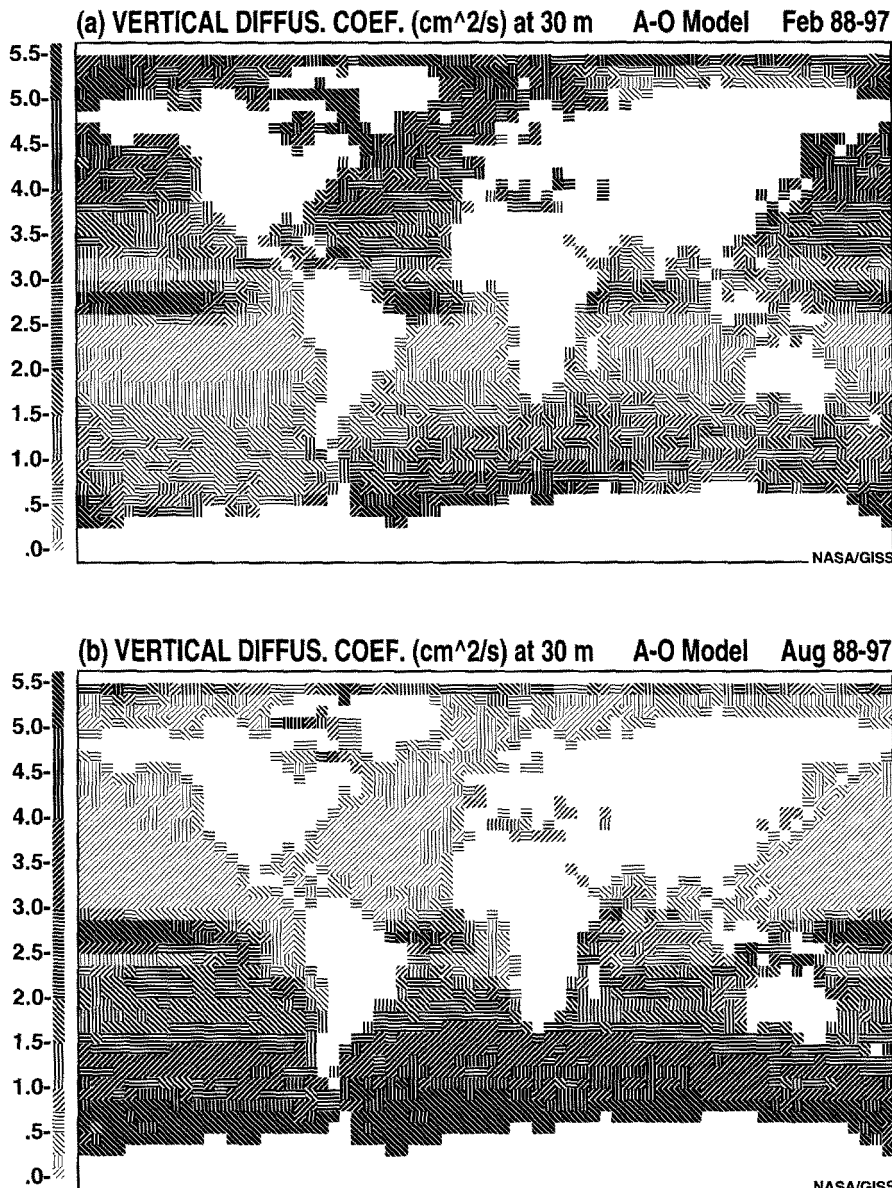


Fig. 16 Vertical diffusion coefficient ( $\text{cm}^2/\text{s}$ ) at 30 m for years 88–97 of the coupled model simulation for (a) February and (b) August.

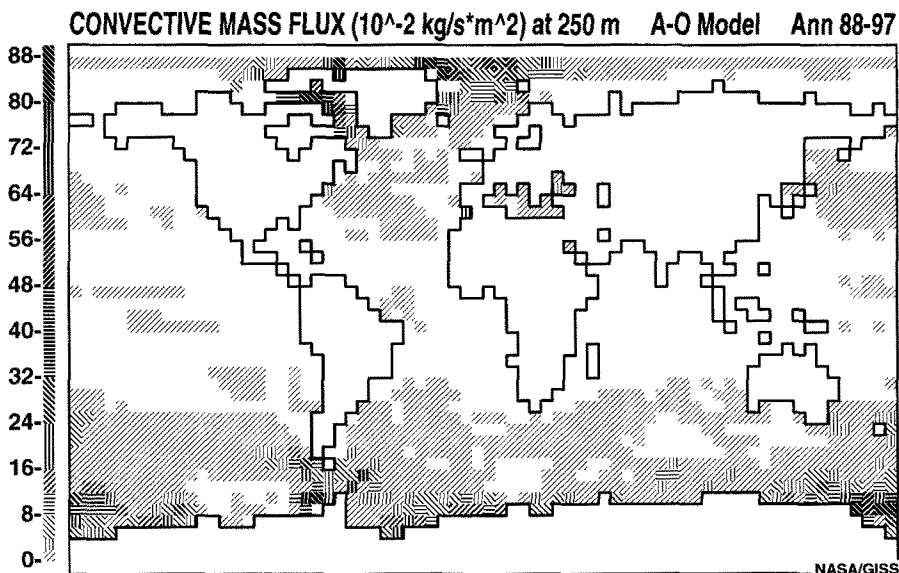


Fig. 17 Annual convective mass flux ( $10^{-2} \text{ kg/s m}^2$ ) at 250 m for years 88–97 of the coupled model simulation.

In some regions stronger vertical diffusion would help eliminate discrepancies, although it would likely have a negative impact on the ability to maintain the seasonal thermocline.

The annual convective mass flux at 250 m is presented in Fig. 17. Vertical overturning is occurring east of Greenland and in the Arctic Ocean, as well as along the Antarctic continent. While observations of this process are not available, the mixing probably is underestimated in the region south of Greenland and in the southern ocean, consistent with the weaker than expected thermohaline circulations in these areas. These are, however, regions which are actually too cold at the surface (Fig. 12), so any underestimation of convection would have to be associated with discrepancies in the salinity field, discussed in Section 3c.

An additional component which can lead to climate drift and can affect vertical mixing is the sea ice field. Model results are compared with observations in Fig. 18. Model sea ice cover is generally less than observed (and therefore could have an impact on convection east and south of Greenland), although this state is arrived at differently in the two hemispheres. Fig. 19 shows the sea ice change as a function of time. In the Northern Hemisphere the sea ice cover, after an initial reduction is very stable, with a slow climb back to the original percentages. In the Southern Hemisphere, sea ice cover oscillates, having been too large during the middle of the experiment. Martinson (1993) argues that very high vertical resolution is needed to properly model southern ocean sea ice due to the marginal stability of the system. In addition, off-line studies indicate that advection of sea ice and the fresh water

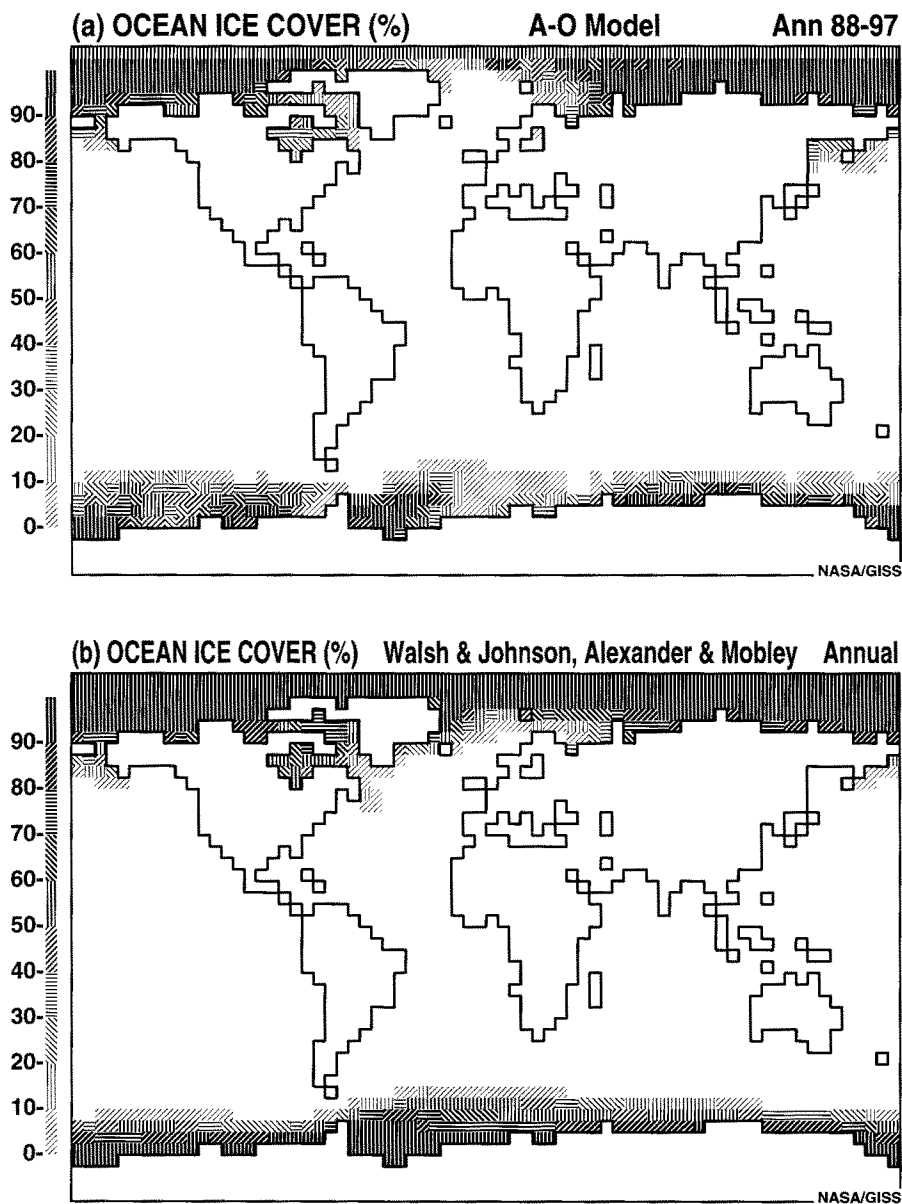


Fig. 18 Annual distribution of sea ice (%) for (a) years 88–97 of the coupled model simulation and (b) observations of Walsh and Johnson (1979) in the Northern Hemisphere and Alexander and Mobley (1976) in the Southern Hemisphere.

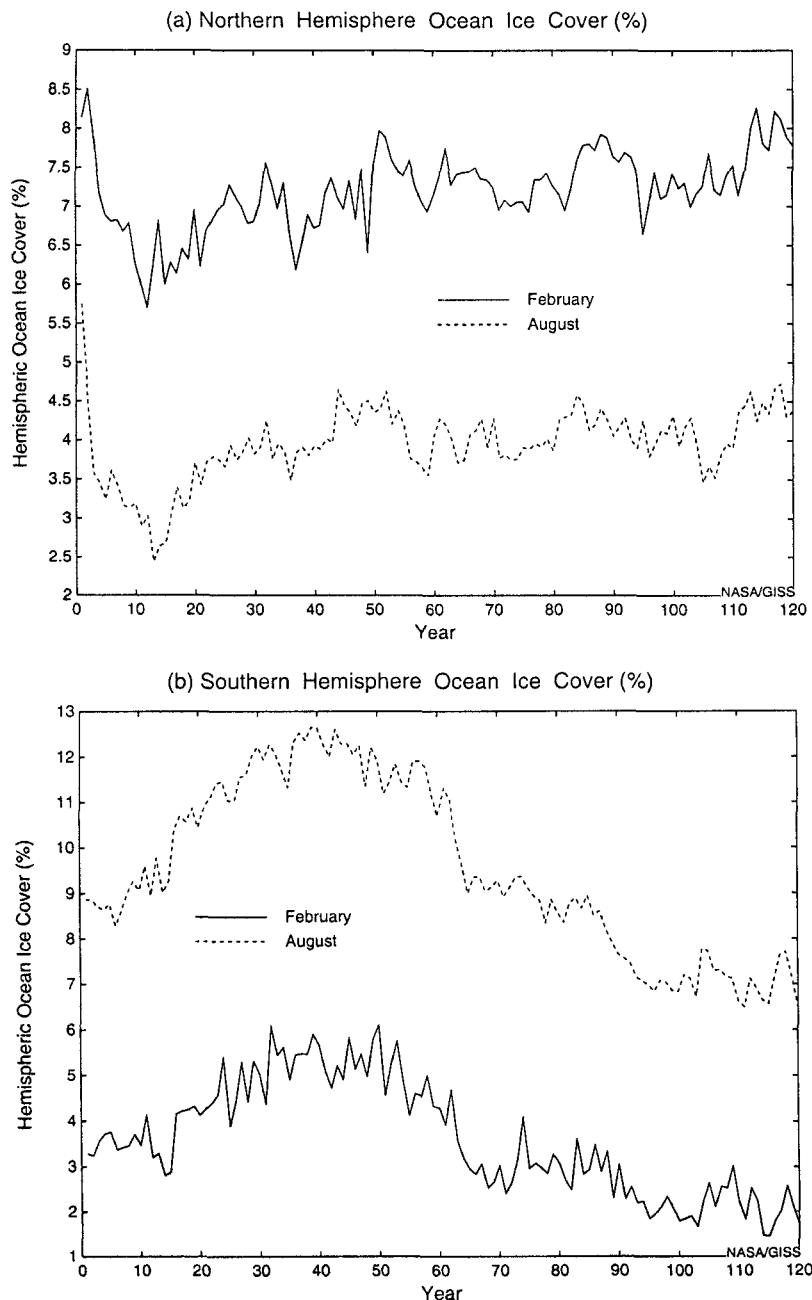


Fig. 19 Hemispheric fraction of sea ice (%) for each year of the coupled model simulation for (a) Northern Hemisphere and (b) Southern Hemisphere.

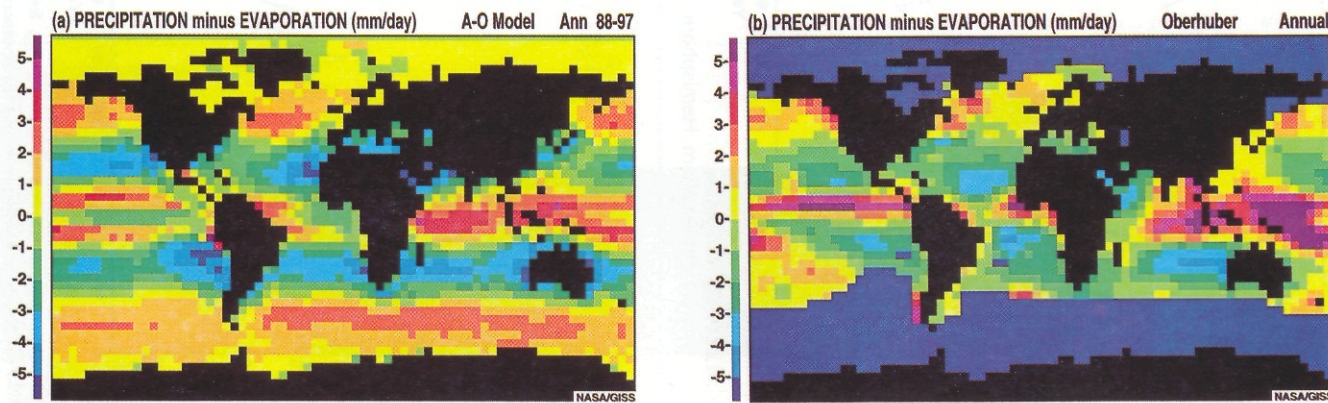
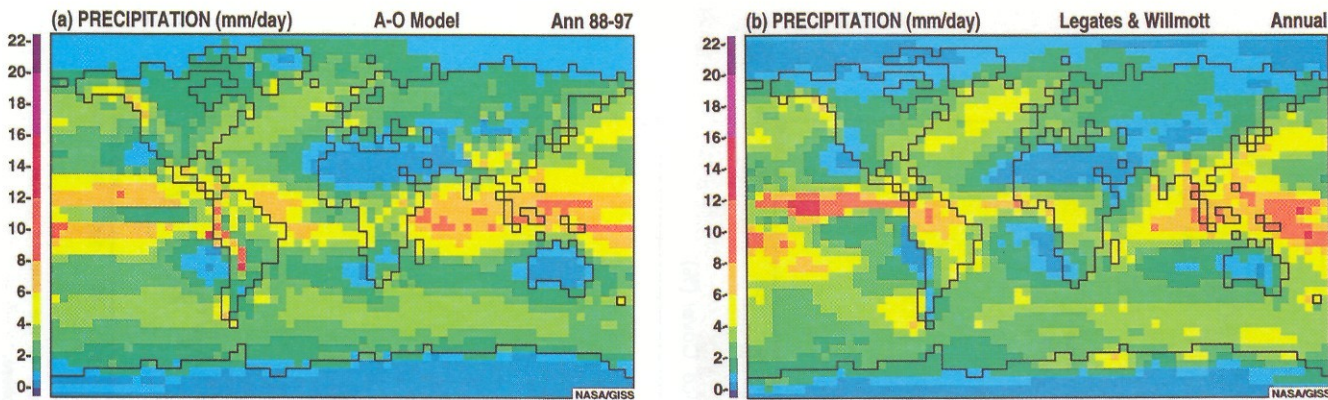


Fig. 22 Annual precipitation minus evaporation (mm/day) for (a) years 88–97 of the coupled model simulation and (b) observations of Oberhuber (1988).

contribution of calving, neither of which are included in this model, improve the Southern ocean sea ice distribution.

### c Model hydrologic properties

The comparison of the model's precipitation with observations is shown in Fig. 20. The general patterns of minimum precipitation in the subtropics with maximum values in the western tropical Pacific, in the Amazon and along storm track positions are simulated in the model. The model's precipitation is too weak along the Inter-Tropical Convergence Zone (ITCZ) and too strong along the western portions of continents in the subtropics (a response to the warmer sea surface temperatures). We note that discrepancies between different observed data sets can be as large as the model deviations.

The model's evaporation is presented in Fig. 21, compared with observations. Subtropical maxima and high latitude minima exist as expected. The model's values appear too large in the subtropical oceans; however, the "observations" are based on specific drag formulations, which differ somewhat from those employed in this model, so a detailed comparison is somewhat questionable. In fact, the "observations" of Baumgartner and Reichel (1975) are somewhat closer to the model in this respect.

The annual net water flux from precipitation minus evaporation and comparison with observations is given in Fig. 22. The flux is positive in the tropics and at high latitudes and negative near the sinking branch of the Hadley cell. Taking the observed values at face value, it would appear that the model provides excess fresh water to the central North Atlantic from 40°–60°N, of up to 1–2 mm d<sup>-1</sup>. Fresh water flux adjustments of this magnitude, or larger, are used in other coupled ocean-atmosphere models (Gates et al., 1993).

The model allows the precipitation over the continents to run into the oceans with the proper seasonal distribution (Miller et al., 1994). The mass outflow by rivers is given in Fig. 23, and a comparison with observations presented in Table 10 (the letters in Fig. 23 correspond to the first letter of the rivers in the table). The quality of the model simulation varies widely, with examples of underestimation of the runoff, often at low latitudes (e.g. the Amazon, the Congo and the Orinoco), examples of overestimation, often at high latitudes (Yukon, McKenzie) and some realistic results (Yenesei, Mississippi, Amur). In particular, for the rivers flowing into the Arctic, the model values are about 30% too large (compared with the study of Agaard and Carmack (1989)). In addition, the model does not allow for advection of sea ice out of the Arctic and its fresh water flow from the Arctic into the North Atlantic is underestimated by at least a factor of two; the combination of these discrepancies lead to a fresh water excess of as much as 1 mm d<sup>-1</sup> for the Arctic and a deficiency of about 0.4 mm d<sup>-1</sup> for the North Atlantic.

The ocean surface salinity is presented in Figs 24a,b. The model produces the expected salinity maxima in the subtropics with relative minima in the equatorial region, and absolute minima at high latitudes. A major discrepancy is that the

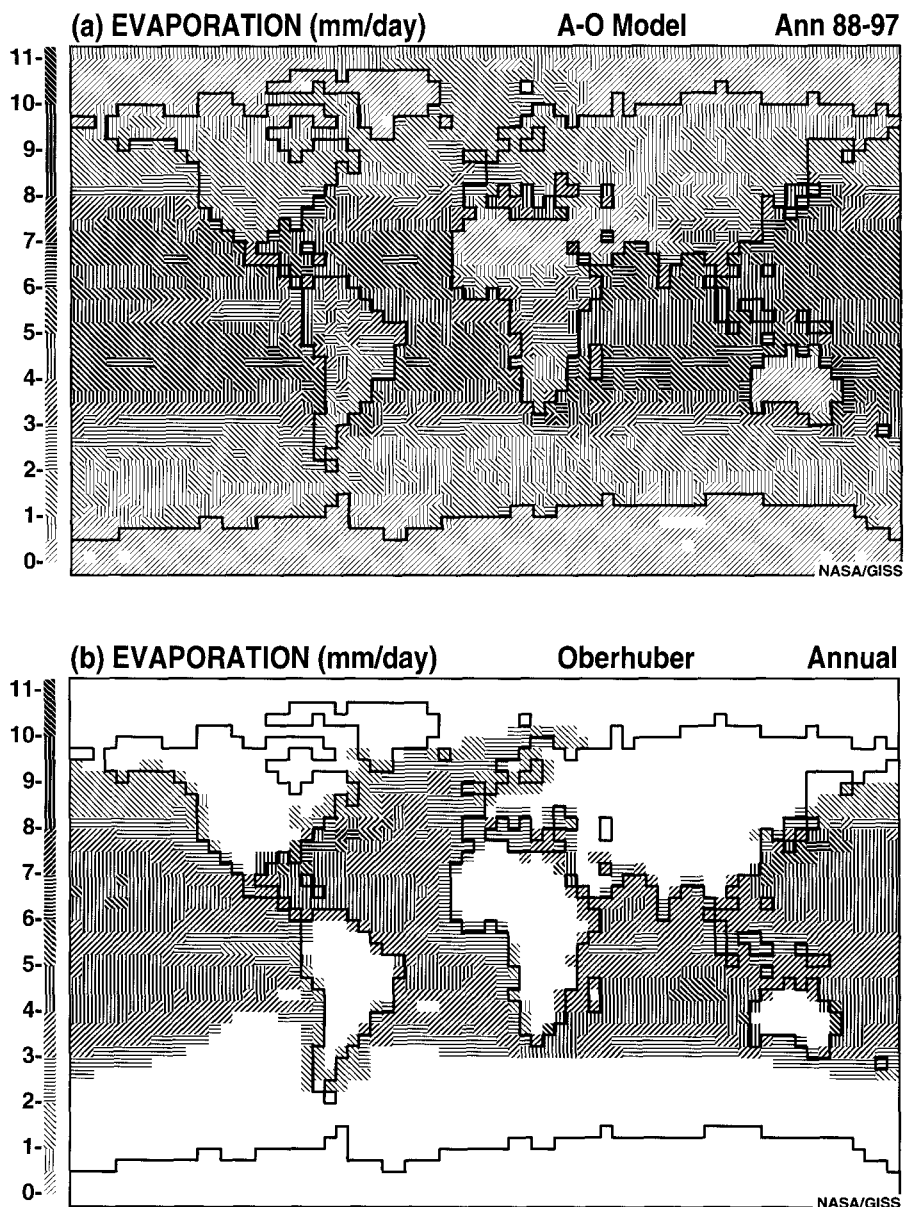


Fig. 21 Annual evaporation (mm/day) for (a) years 88–97 of the coupled model simulation and (b) observations of Oberhuber (1988).

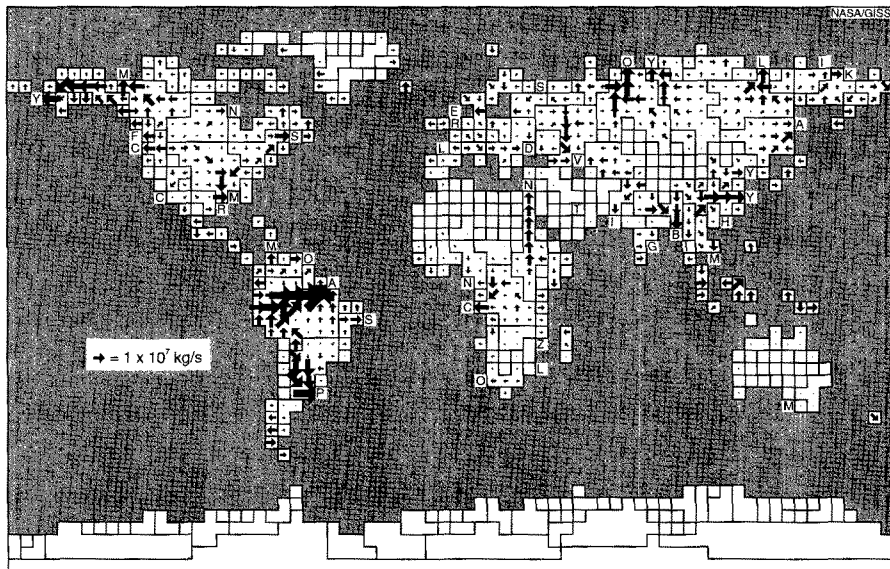


Fig. 23 Annual mass outflow by rivers for years 88-97 of the coupled model simulation. The mouths of major rivers are indicated by the first letter of the river's name, which are listed in Table 10. The area of the arrows is proportional to the flow.

model salinity is too low in the North Atlantic south of Greenland. This error is consistent with reduced values of NADW formation poleward of 30°N. A review of the results in Figs 20-23 suggests that the low salinity is associated with the reduced evaporation (Fig. 21). Note that a positive feedback occurs; with reduced evaporation, the salinity is too low, the North Atlantic overturning circulation too weak, less mass, heat and salt are transported poleward (as discussed in conjunction with Fig. 6, the Gulf Stream transport is probably some 45% too weak, being too eastward as opposed to northeastward in this region). With less heat transport converging in this region, temperatures are too cold (Fig. 12) and evaporation too weak. The problem could be initiated by errors in precipitation, sea ice formation, or the inadequate resolution of the model affecting ocean transports and dynamics. This particular problem, which is common to other models, is one that flux adjustments are specifically designed to correct. Overall, the model's global rms surface salinity deviation from the Levitus (1982) climatology is 0.97 per mil. Note that despite the calculated freshwater imbalance for the Arctic, the salinity is only slightly lower than in the observations.

The model is accumulating moisture over Antarctica and Greenland. For Antarctica the snow accumulation is at a rate of  $174 \text{ kg m}^{-2} \text{ yr}^{-1}$ , while for Northern Hemisphere ice caps the value is  $17 \text{ kg m}^{-2} \text{ yr}^{-1}$ . These results caused mean sea

TABLE 10. Annual river flow (Sv) of the Earth's principal rivers for years 88–97 of the climate model simulation and for the observations of Milliman and Meade (1983).

Observation	Model	River
0.1998	0.0748	Amazon
0.0103	0.0119	Amur
0.0308	0.0170	Brahmaputra+Ganges
0.0006	0.0031	Colorado
0.0080	0.0131	Columbia
0.0397	0.0170	Congo
0.0065	0.0053	Danube
0.0020	0.0017	Elbe
0.0007	0.0003	Fraser
0.0027	0.0020	Godavari
0.0096	0.0027	Hsi Chiang
0.0017	0.0038	Indigirka
0.0075	0.0053	Indus
0.0136	0.0025	Irrawady
0.0023	0.0120	Kolyma
0.0163	0.0173	Lena
0.0002	0.0001	Limpopo
0.0	0.0019	Loire
0.0097	0.0207	Mackenzie
0.0075	0.0046	Magdalena
0.0149	0.0085	Mekong
0.0184	0.0171	Mississippi
0.0007	0.0003	Murray
0.0061	0.0027	Niger
0.0026	0.0098	Nile
0.0122	0.0210	Ob
0.0003	0.0024	Orange
0.0349	0.0101	Orinoco
0.0149	0.0416	Parana (LaPlata)
0.0	0.0037	Rhine
0.0	0.0033	Rio Grande
0.0031	0.0070	Sao Francisco
0.0033	0.0043	Severnaya Divina
0.0142	0.0096	St. Lawrence
0.0015	0.0015	Tigris-Euphrates
0.0134	0.0050	Volga
0.0285	0.0179	Yangtze (Changjiang)
0.0016	0.0065	Yellow (Huanghe)
0.0178	0.0178	Yenesei
0.0062	0.0253	Yukon
0.0071	0.0005	Zambesi

level to drop at a rate of  $6.73 \text{ mm year}^{-1}$ . The sea level change is a problem which cannot be solved by flux adjustments, as it involves the atmospheric physics and cryospheric dynamics (calving, a major mechanism for Antarctic ice sheet mass loss, is not included in any coupled atmosphere-ocean model). For example, the UKMO coupled model, with flux adjustments, produces an almost identical imbalance, with sea level dropping at a rate of  $6.6 \text{ mm year}^{-1}$  (Gregory, 1993). In fact,

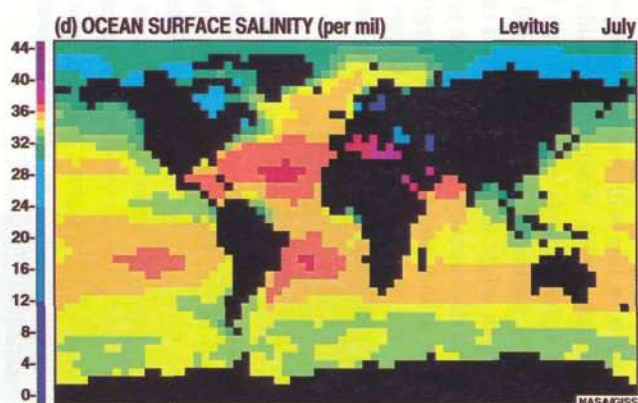
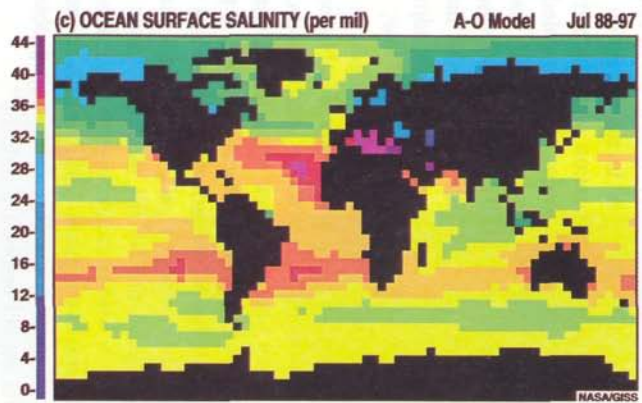
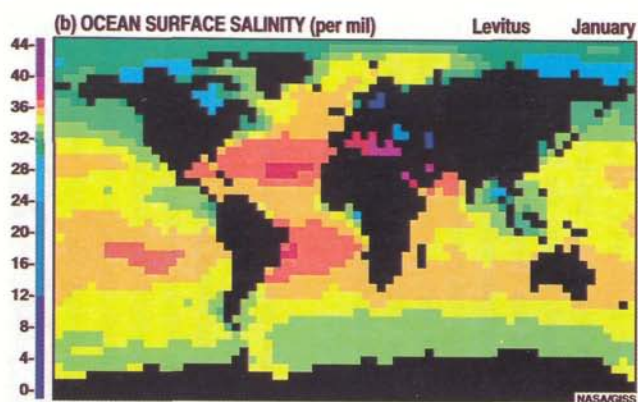
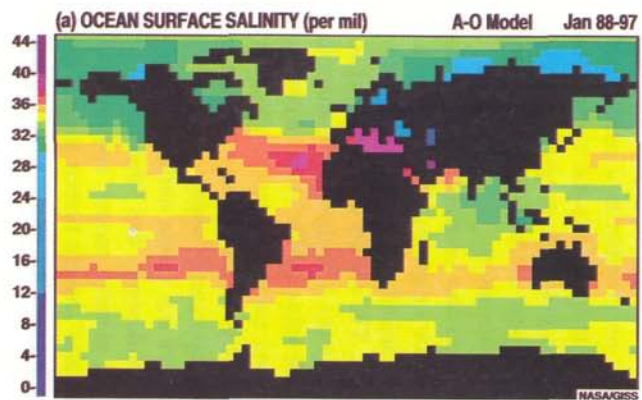


Fig. 24 Ocean surface salinity (per mil) for (a) years 88–97 of the coupled model simulation for January; (b) observations of Levitus (1982) for January; (c) the coupled model simulation for July, and (d) observations of Levitus for July.

as noted by Gregory, this figure for water mass accumulation over Antarctica and Greenland is in line with current estimates of accumulation (IPCC, 1990; Fortuin and Oerlemans 1990). Whether it invalidates use of the model for sea-level change estimates again depends on the problem being addressed. During the last century sea level is estimated to have increased by about 12 cm (Gornitz and Hansen, 1982), which might well be too small a change to investigate with a model having this large a discrepancy. Future climate sea level change estimates are of a similar magnitude to the model imbalance; Gregory (1993) felt that assessments were still possible. We note that additional factors, such as the inclusion of all substantial mountain glaciers, will also affect the accuracy of model sea level projections.

#### 4 Discussion and Conclusions

The coupled model described above introduces a new dynamical ocean model in conjunction with a version of the GISS atmospheric model. The major new feature is the use of the linear upstream scheme for heat, moisture and salt advection, replacing the commonly used second order advection scheme which produces considerable numerical noise. This eliminates the need for explicit horizontal or vertical diffusion for numerical stability. It also provides an implicitly higher resolution for advection of heat, moisture and salt, also reducing the need for large vertical diffusion values. The model can thus maintain a stable thermocline structure for at least one century.

Additional distinctive features include the simultaneous coupling of atmosphere and ocean fluxes (every hour), the incorporation of the twelve straits, allowing for passage of water in locations which would not be possible in a coarse grid model and the incorporation of surface river flow from the land to the ocean with the proper seasonal timing. The coupled model also has been programmed for maximum time efficiency: at  $4^\circ \times 5^\circ$  resolution one-year model simulation takes about one day on the IBM RISC 6000 model 590 workstation.

The model is run without the use of flux adjustments and several features could undoubtedly be improved were such adjustments to be employed. The salinity in the northern North Atlantic is too low; a positive salinity flux should intensify North Atlantic Deep Water production in this region. The results of Manabe et al. (1991) demonstrate that a considerably broader and more vigorous North Atlantic circulation is possible with a judicious choice of such adjustments. The other major deficiency relates to lack of sufficient wind stress and associated upwelling in the eastern portions of the tropical oceans, a problem compounded by the reduction in marine stratus which arises when the sea surface temperatures warm.

Meehl (in Gates et al., 1993) notes that the choice not to use surface flux adjustments (in the NCAR model) is made with the philosophy that "the display of errors is a useful measure of the deficiencies of the coupled model, and provides an informative context within which to interpret results". Meehl further states, "the best solution to the flux correction problem is to improve the component models so that model errors are reduced".

In that regard, various model improvements are under way. A new atmospheric model is nearing completion at GISS, which has, among other things, a more realistic Hadley circulation. This should improve upwelling along the tropical coasts. The model is also in approximate radiation balance (with the help of a small solar constant reduction), which should limit the climate drift (of  $0.006^{\circ}\text{C}$  year $^{-1}$  in the surface air temperature) that occurs in this model; alterations in the ocean albedo would also help provide better radiation balance. Prospective additions to the ocean model include advection of sea ice, which in off-line studies have improved the Southern Hemisphere sea ice simulations and may impact Antarctic Bottom Water formation, and the inclusion of an ice calving contribution in that region. Sea ice advection also plays an important role in the water balance for the Arctic and North Atlantic. We are exploring the possibility of running the ocean model at finer horizontal resolution (when coupled to the new atmosphere model, the ocean model will take just 15% of the total computer time, with both at  $4^{\circ} \times 5^{\circ}$  resolution).

Tziperman et al. (1994) emphasize that the instability of the thermohaline circulation is sensitive to the flux adjustments used, in the sense that with a shorter time lag restoring force, and hence larger flux adjustments, the control run ocean is closer to being unstable. Ocean circulation instabilities are a possibility for the warming climate of the next century, and in fact have been found in several different models; thus a prime reason for developing coupled models without flux adjustments is to guarantee that climate change results are not a function of the flux adjustments (and that this important component of the system is being given the proper degrees of freedom). This model has been used to simulate the climate associated with a 1% compound annual increase of CO<sub>2</sub>, in conjunction with the latest IPCC experiments. Both the control run and climate change diagnostic output have been provided to the IPCC and are available on GISS's World Wide Web site at "<http://www.giss.nasa.gov/Data/>".

The coupled model described here is available for testing and utilization by the scientific community; those interested in obtaining a copy of the code should contact G. Russell.

### Acknowledgments

A complex atmosphere-ocean model requires contributions from many individuals. Various people, who contributed to the development and analysis of this atmosphere-ocean model or to this paper, directly or indirectly, are listed in alphabetical order: Frank Abramopoulos, James Bishop, Anthony Broccoli, Kirk Bryan, Guilherme Caliri, Mark Cane, Mark Chandler, Anthony Del Genio, Keith Dixon, Inez Fung, Dale Haidvogel, James Hansen, Xingjian Jiang, Andrew Lacis, Jean Lerner, Jochem Marotzke, Douglas Martinson, Syukuro Manabe, Ernst Maier-Reimer, Paulo Malanotte-Rizzoli, Anthony Rosati, Cynthia Rosenzweig, William Rossow, Reto Ruedy, Peter Stone, Robert Suozzo, and Hanspeter Zinn.

Model development support was provided by the NASA Climate Program Office, by the Earth Observing System interdisciplinary funding, and by the United States

Environmental Protection Agency office by Policy, Planning and Evaluation, Global Climate Division.

## References

- AAGAARD, K. and E.C. CARMACK. 1989. The role of sea ice and other fresh water in the Arctic circulation. *J. Geophys. Res.* **94**: 14485–14498.
- ALEXANDER, R.C. and R.L. MOBLEY. 1976. Monthly average sea-surface temperatures and ice-pack limits on a 1% global grid. *Mon. Weather Rev.* **104**: 143–148.
- ARAKAWA, A. and V.R. LAMB. 1977. Computational design of the basic dynamical processes of the UCLA general circulation model. In: *Methods in Computational Physics*, Vol. 17, Academic Press. 337. pp.
- BARKER, H.W.; Z. LI and J.-P. BLANCHET. 1994. Radiative characteristics of the Canadian Climate Centre, second-generation general circulation model. *J. Clim.* **7**: 1070–1091.
- BAUMGARTNER, A. and E. REICHEL. 1975. *The World Water Balance*. Elsevier, Amsterdam, 179 pp.
- BISHOP, J. and W. ROSSOW. 1991. Spatial and temporal variability of global surface solar irradiance. *J. Geophys. Res.* **96**: 16839–16858.
- BOER, G.J.; N.A. MCFARLANE, J.-P. BLANCHET and M. LAZARE. 1992. The Canadian Climate Centre second-generation general circulation model and its equilibrium climate. *J. Clim.* **5**: 1031–1044.
- BRYAN, F. 1987. Parameter sensitivity of primitive equation ocean general circulation models. *J. Phys. Oceanogr.* **17**: 970–985.
- BRYAN, K. and L.J. LEWIS. 1979. A water mass model of the world ocean. *J. Geophys. Res.* **84**: 2503–2517.
- CALLAHAN, P.S. 1993. The TOPEX/Poseidon GDR Users Handbook. Doc. D-8944 Rev. B, Jet Propul. Lab., Pasadena, Cal., 84 pp.
- DRUYAN, L.M.; K.-W.K. LO, K.P. SHAH, J.A. MARENGO and G.L. RUSSELL. 1994. Impacts of model improvements on GCM sensitivity to SST forcing. *Int. J. Climatol.*, submitted.
- ENGLAND, M.H. 1993. Representing the global-scale water masses in ocean general circulation models. *J. Phys. Oceanogr.* **23**: 1523–1552.
- ESBENSEN, S.K. and Y. KUSHNIR. 1981. The heat budget of the global ocean: an atlas based on estimates from surface marine observations. Climate Research Institute, Oregon State University, Corvallis, Ore.
- FORTUIN, J.P.F. and J. OERLEMANS. 1990. Parameterization of the annual surface temperature and mass balance of Antarctica. *Ann. Glaciol.* **14**: 78–84.
- GATES, W.L.; U. CUBASCH, G.A. MEEHL, J.F.B. MITCHELL and R.J. STOUFFER. 1993. An intercomparison of selected features of the control climates simulated by coupled ocean-atmosphere general circulation models. World Climate Programme, WCRP-82, World Meteorological Organization, WMO/TD - No. 574, 46 pp.
- GORNITZ, V.; S. LEBEDEFF and J. HANSEN. 1982. Global sea level trend in the past century. *Science* **215**: 1161–1164.
- GREGORY, J.M. 1993. Sea-level changes under increasing atmospheric CO<sub>2</sub> in a transient coupled ocean-atmosphere GCM experiment. *J. Clim.* **6**: 2247–2262.
- HALKIN, D. and T. ROSSBY. 1985. The structure and transport of the Gulf Stream at 73°W. *J. Phys. Oceanogr.* **15**: 1439–1452.
- HALL, M.M. and H.L. BRYDEN. 1982. Direct estimates and mechanisms of ocean heat transport. *Deep-Sea Res.* **29**: 339–359.
- HANSEN, J.; I. FUNG, A. LACIS, S. LEBEDEFF, D. RIND, R. RUEDY and G. RUSSELL. 1988. Global climate changes as forecast by the Giss 3-D model. *J. Geophys. Res.* **92**: 14739–14760.
- ; A. LACIS, D. RIND, G. RUSSELL, P. STONE, I. FUNG, R. RUEDY and J. LERNER. 1984. Climate sensitivity: Analysis of feedback mechanisms. In: *Climate Processes and Climate Sensitivity*, *Geophys. Monogr. Ser.*, Vol. 29, J.E. Hansen and T. Takahashi (Eds), AGU, Washington, D.C. pp. 130–163.
- ; G. RUSSELL, D. RIND, P. STONE, A. LACIS, S. LEBEDEFF, R. RUEDY and L. TRAVIS. 1983. Efficient three-dimensional global models for climatic studies: Models I and II. *Mon. Weather Rev.* **111**: 609–662.
- HASTENRATH, S. 1980. Heat budget of tropical ocean and atmosphere. *J. Phys. Oceanogr.* **10**: 159–170.
- HELLERMAN, S. and M. ROSENSTEIN. 1983. Normal monthly wind stress over the world ocean with error estimates. *J. Phys. Oceanogr.* **13**: 1093–1104.

# An Atmosphere-Ocean Model for Climate Change Studies / 729

- HOUGHTON, J.T.; G.J. JENKINS and J.J. EPHRAUMS 1990. *Climate Change. The IPCC Scientific Assessment*, Cambridge University Press, U.K., 365 pp.
- ; B.A. CALLANDER and S.K. VARNEY 1992. *Climate Change 1992*, Cambridge University Press, U.K., 200 pp.
- JIANG, X. and I. FUNG. 1994. Ocean response to surface heat anomalies. *J. Clim.* 7: 783–791.
- JOYCE, T.M. and W.J. SCHMITZ. 1988. Zonal velocity structure and transport in the Kuroshio Extension. *J. Phys. Oceanogr.* 18: 1484–1494.
- KILLWORTH, P.D.; D. STAINFORTH, D.J. WEBB and S.M. PATERSON. 1991. The development of a free-surface Bryan-Cox-Semtner ocean model. *J. Phys. Oceanogr.* 21: 1333–1348.
- LEGATES, D. and C. WILLMOTT. 1990. Mean seasonal and spatial variability in gauge-corrected global precipitation. *Int. J. Climatol.* 10: 111–128.
- LEVITUS, S. 1982. Climatological Atlas of the World Ocean. Prof. pap. 13, NOAA, U.S. Govt. Printing Office, Washington, DC, 173 pp.
- MAIER-REIMER, E. and K. HASSELMANN. 1987. Transport and storage of CO<sub>2</sub> in the ocean: an inorganic ocean-circulation carbon cycle model. *Clim. Dyn.* 2: 63–90.
- MANABE, S.; M.J. SPELMAN and R.J. STOUFFER. 1992. Transient responses of a coupled ocean-atmosphere model to gradual changes of atmospheric CO<sub>2</sub>, part II: seasonal response. *J. Clim.* 5: 105–126
- ; R.J. STOUFFER, M.J. SPELMAN and K. BRYAN. 1991. Transient responses of a coupled ocean-atmosphere model to gradual changes of atmospheric CO<sub>2</sub>. Part I: annual mean response. *J. Clim.* 4: 785–818.
- MARTINSON, D. 1993. Ocean heat and sea ice thicknesses in the southern ocean. In: *Ice in Climate*, W. Peltier (Ed.), NATO, in press.
- MEEHL, G.A. 1990. Seasonal cycle forcing of El Niño–Southern Oscillation in a global, coupled ocean-atmosphere GCM. *J. Clim.* 3: 72–98.
- ; G.W. BRANSTRATOR and W.M. WASHINGTON. 1993a. Tropical Pacific interannual variability and CO<sub>2</sub> climate change. *J. Clim.* 6: 42–63.
- and W.M. WASHINGTON. 1993. South Asian summer monsoon variability in a model with doubled atmospheric carbon dioxide concentrations. *Science* 260: 1101–1104.
- ; — and T.R. KARL. 1993b. Low-frequency variability and CO<sub>2</sub> transient climate change. Part 1. Time-averaged differences. *Clim. Dyn.* 8: 117–133.
- MILLER, J.R.; G.L. RUSSELL and G. CALIRI. 1994. Continental scale river flow in climate models. *J. Clim.* 7: 914–928.
- MILLIMAN, J.D. and R.H. MEADE. 1983. World-wide delivery of river sediment to the oceans. *J. Geol.* 91(1): 1–21.
- MURPHY, J.M. 1992. A prediction of the transient response of climate. Climate Research Technical Note 32, Hadley Centre for Climate Prediction and Research, Bracknell, 27 pp.
- NOWLIN, W.D. and J.M. KLINCK. 1986. The physics of the Antarctic Circumpolar Current. *Rev. Geophys.* 24: 469–491.
- OBERHUBER, J.M. 1988. An atlas based on the 'COADS' data set: the budgets of heat, buoyancy and turbulent kinetic energy at the surface of the global ocean. Max-Planck-Institute for Meteorology, Report No. 15, Hamburg, Germany, 198 pp.
- OERT, A.H. and T.H. VONDER HAAR. 1976. On the observed annual cycle in the ocean-atmosphere heat balance over the Northern Hemisphere. *J. Phys. Oceanogr.* 6: 781–800.
- PACANOWSKI, R.C. and S.G.H. PHILANDER. 1981. Parameterization of vertical mixing in numerical models of tropical oceans, *J. Phys. Oceanogr.* 11: 1443–1451.
- PAULSON, C.A. and J.J. SIMPSON. 1977. Irradiance Measurements in the upper ocean. *J. Appl. Oceanogr.* 7: 952–956.
- PETERSON, R.G. 1988. On the transport of the Antarctic Circumpolar Current through Drake Passage and its relation to wind. *J. Geophys. Res.* 93: 13993–14004.
- PRATHER, M.J. 1986. Numerical advection by conservation of second order moments. *J. Geophys. Res.* 91: 6671–6680.
- ROBINSON, M.K. and R.A. BAUER. 1982. Sea-surface temperature climatology. Oceanographic Monthly Summary S. Auer (Ed.), NOAA, Boulder, Colo., April.
- ROSSOW, W.B. and Y.-C. ZHANG. 1995. Calculation of surface and top-of-atmosphere radiative fluxes from physical quantities based on ISCCP datasets: 2. Validation and first results. *J. Geophys. Res.* 100: 1167–1197.
- RUSSELL, G.L. and J.A. LERNER. 1981. A new finite-differencing scheme for the tracer transport equation. *J. Appl. Meteorol.* 20: 1483–1498.
- ; J.R. MILLER and L.-C. TSANG. 1985. Seasonal oceanic heat transports computed from an atmospheric model. *Dyn. Atmos. Oceans* 9: 253–271.

- SAUSEN, R.; K. BARTHEL and K. HASSELMANN. 1988. Coupled ocean-atmosphere models with flux correction. *Clim. Dyn.* **2**: 145–164.
- SEMTNER, A.J. and R.M. CHERVIN. 1992. Ocean general circulation from a global eddy-resolving model. *J. Geophys. Res.* **97**: 5493–5550.
- SHAPIRO, R. 1970. Smoothing, filtering and boundary effects. *Rev. Geophys. Space Phys.* **8**: 359–387.
- STAMMER, D. and C. WUNSCH. 1994. Preliminary assessment of the accuracy and precision of TOPEX/POSEIDON altimeter data with respect to the large-scale ocean circulation. *J. Geophys. Res. Oceans* **99**: 24584–24604.
- TAU, C.-K. 1988. Estimating the basin-scale ocean circulation from satellite altimetry. Part I: Straightforward spherical harmonic expansion. *J. Phys. Oceanogr.* **18**: 1398–1413.
- TRENBERTH, K.E. 1979. Mean annual poleward energy transports by the oceans in the Southern Hemisphere. *Dyn. Atmos. Oceans*, **4**: 57–64.
- TSELILOUDIS, G.; W.B. ROSSOW and D. RIND. 1992. Global patterns of cloud optical thickness variation with temperature. *J. Clim.* **5**: 1484–1495.
- TZIPERMAN, E.; J.R. TOGGWEILER, Y. FELIKS and K. BRYAN. 1994. Instability of the thermohaline circulation with respect to mixed boundary conditions: is it really a problem for realistic models? *J. Phys. Oceanogr.* **24**: 217–232.
- WALSH, J. and C. JOHNSON. 1979. An analysis of Arctic sea ice fluctuations. *J. Phys. Oceanogr.* **9**: 580–591.
- WASHINGTON, W.M. and G.A. MEEHL. 1989. Climate sensitivity due to increased CO<sub>2</sub>: experiments with a coupled atmosphere and ocean general circulation model. *Clim. Dyn.* **4**: 1–38.
- ; —, L. VERPLANK and T.W. BETTGE. 1994. A world ocean model for greenhouse sensitivity studies: resolution intercomparison and the role of diagnostic forcing. *Clim. Dyn.* **9**: 321–344.
- WHITWORTH, T. 1993. Monitoring the transport of the Antarctic Circumpolar Current at Drake Passage, *J. Phys. Oceanogr.* **13**: 2045–2057.
- and R.G. PETERSON. 1985. The volume transport of the Antarctic Circumpolar Current from bottom pressure measurements. *J. Phys. Oceanogr.* **15**: 810–816.
- ZHANG, Y.-C.; W.B. ROSSOW and A.A. LACIS. 1995. Calculation of surface and top-of-atmosphere radiative fluxes from physical quantities based on ISCCP datasets: 1. Method and sensitivity to input data uncertainties. *J. Geophys. Res.* **100**: 1149–1165.